

AperTO - Archivio Istituzionale Open Access dell'Università di Torino

Chlorine-rich metasomatic H₂O-CO₂ fluids in amphibole-bearing peridotites from Injibara (Lake Tana region, Ethiopian plateau): nature and evolution of volatiles in the mantle of a region of continental flood basalts.

This is the author's manuscript

Original Citation:

Availability:

This version is available <http://hdl.handle.net/2318/133025> since

Published version:

DOI:10.1016/j.gca.2010.02.007

Terms of use:

Open Access

Anyone can freely access the full text of works made available as "Open Access". Works made available under a Creative Commons license can be used according to the terms and conditions of said license. Use of all other works requires consent of the right holder (author or publisher) if not exempted from copyright protection by the applicable law.

(Article begins on next page)



UNIVERSITÀ DEGLI STUDI DI TORINO

This Accepted Author Manuscript (AAM) is copyrighted and published by Elsevier. It is posted here by agreement between Elsevier and the University of Turin. Changes resulting from the publishing process - such as editing, corrections, structural formatting, and other quality control mechanisms - may not be reflected in this version of the text. The definitive version of the text was subsequently published in *Geochimica et Cosmochimica Acta*, 74, 10, 2010, doi:10.1016/j.gca.2010.02.007.

You may download, copy and otherwise use the AAM for non-commercial purposes provided that your license is limited by the following restrictions:

- (1) You may use this AAM for non-commercial purposes only under the terms of the CC-BY-NC-ND license.
- (2) The integrity of the work and identification of the author, copyright owner, and publisher must be preserved in any copy.
- (3) You must attribute this AAM in the following format: Creative Commons BY-NC-ND license (<http://creativecommons.org/licenses/by-nc-nd/4.0/deed.en>), doi:10.1016/j.gca.2010.02.007

1 **Chlorine-rich metasomatic H₂O-CO₂ fluids in amphibole-bearing peridotites from**
2 **Injibara (Lake Tana region, Ethiopian plateau): nature and evolution of volatiles in**
3 **the mantle of a region of continental flood basalts**

4
5
6 Maria Luce Frezzotti¹, Simona Ferrando², Angelo Peccerillo³, Maurizio Petrelli³, Francesca Tecce⁴
7 and Andrea Perucchi⁵

8
9 ¹ Department of Earth Sciences, University of Siena, Via Laterina 8, 53100 Siena, Italy.

10 *frezzottiml@unisi.it*

11 ² Department of Mineralogical and Petrological Sciences, University of Torino, Via V. Caluso 35,
12 10125 Torino, Italy.

13 ³ Department of Earth Sciences, University of Perugia, P.zza Università 1, 06100 Perugia, Italy.

14 ⁴ IGAG - CNR, c/o Department of Earth Sciences, University Roma 1 – La Sapienza, P.za A. Moro 5,
15 00185 Roma, Italy.

16 ⁵ Sincrotrone ELETTRA, Trieste, 34012 Basovizza (Trieste), Italy.

17

18 **Abstract**

19 Petrological and geochemical study of volatile bearing phases (fluid inclusions, amphibole,
20 and nominally anhydrous minerals) in a spinel lherzolite xenolith suite from Quaternary lavas at
21 Injibara (Lake Tana region, Ethiopian plateau) shows compelling evidence for metasomatism in the
22 lithospheric mantle in a region of mantle upwelling and continental flood basalts. The xenolith
23 suite consists of deformed (i.e., protogranular to porphyroclastic texture) Cl-rich pargasite
24 lherzolites, metasomatized (LILE, and Pb enrichment in clinopyroxene and amphibole) at $T \leq$
25 1000°C . Lherzolites contain chlorine-rich $\text{H}_2\text{O}-\text{CO}_2$ fluid inclusions, but no melt inclusions. Fluid
26 inclusions are preserved only in orthopyroxene, while in olivine, they underwent extensive
27 interaction with host mineral. The metasomatic fluid composition is estimated: $X_{\text{CO}_2} = 0.64$, $X_{\text{H}_2\text{O}} =$
28 0.33 , $X_{\text{Na}} = 0.006$, $X_{\text{Mg}} = 0.006$, $X_{\text{Cl}} = 0.018$, (salinity = 14 - 10 NaCl eq. wt. %, $a_{\text{H}_2\text{O}} = 0.2$, Cl = 4-5
29 mole %). Fluid isochores correspond to trapping pressures of 1.4 - 1.5 GPa or 50 -54 km depth (at
30 $T = 950^{\circ}\text{C}$). Synchrotron sourced micro-infrared mapping (ELECTRA, Trieste) shows gradients for
31 H_2O distribution in nominally anhydrous minerals, with considerable enrichment at grain
32 boundaries, along intragranular microfractures, and around fluid inclusions. Total water amounts
33 in lherzolites are variable from about 150 up to 400 ppm. Calculated trace element pattern of
34 metasomatic fluid phases, combined with distribution and amount of H_2O in nominally anhydrous
35 minerals, delineate a metasomatic Cl-, and LILE-rich fluid phase heterogeneously distributed in the
36 continental lithosphere. Present data suggest that Cl-rich aqueous fluids were important
37 metasomatic agents beneath the Ethiopian plateau, locally forming high water content in the
38 peridotite, which may be easily melted. High Cl, LILE, and Pb in metasomatic fluid phases suggests
39 the contribution of recycled altered oceanic lithosphere component in their source.

40

41 **Keywords:** peridotites, Cl, H_2O , mantle metasomatism, Ethiopian plateau, large igneous province

42 **1. INTRODUCTION**

43

44 C-O-H-S and halogens present in the Earth's upper mantle in different physical states (i.e.
45 free fluid¹ phases, dissolved in melts, in interstitial solid solutions, as well as stored in nominally
46 anhydrous minerals) play a fundamental role in mantle properties and processes, including
47 rheology, metasomatism, and melting (e.g., Wallace and Green, 1988; Thompson, 1992; Green
48 and Falloon, 1998; Wyllie and Ryabchikov, 2000; Dasgupta and Hirschmann, 2006).

49 Fluid inclusions in xenolith suites provide an important opportunity to characterize free
50 fluid phases at depth (cf., Andersen and Neumann, 2001 for a review). Since E. Roedder's first
51 studies (1965), it has been evident that CO₂ dominate in the lithospheric mantle (< 2-3 GPa).
52 Overwhelming CO₂, however, is not the sole component in mantle fluid inclusions. H₂O-bearing
53 CO₂ inclusions have been reported in peridotites from subduction-zones (e.g., Schiano et al., 1995),
54 and, more recently, from Canary and Hawaii intraplate oceanic settings (Frezzotti et al., 2002a and
55 b; Frezzotti and Peccerillo, 2007), revealing a major role for aqueous fluid phases also in zones of
56 intraplate mantle upwelling. At Tenerife (Canary Islands), Frezzotti et al. (2002a) suggested a
57 chlorine-rich composition for aqueous fluids, based on the presence of reaction rims of talc +
58 carbonate + halite lining fluid inclusions. However, a quantification of the halogen (e.g. chlorine)
59 content of aqueous fluid phases at lithospheric depths by fluid inclusion study is missing. Yet, such
60 an information would be of particular interest to trace the H₂O exchanges between Earth's
61 reservoirs, since chlorine is water-soluble and behaves incompatibly. In contrast, at higher
62 pressures, above 4-5 GPa, a high Cl activity in aqueous fluids is testified by hydro-saline fluids (Cl
63 about 12 - 50 mol. %) in sub-micrometer sized inclusions in diamonds (Navon et al., 1988; Izraeli
64 et al., 2001; Klein-BenDavid et al., 2004; 2007) .

65 Present study aims to provide a better understanding of the role of volatiles in the
66 lithosphere of a region of continental mantle upwelling and formation of large igneous provinces
67 (LIP's). LIP's are traditionally interpreted as melting products of plume heads (White and McKenzie,
68 1995; Condie, 2001; Ernst and Buchan, 2003), although the relative lithospheric – plume
69 contribution to the extensive magmatism are debated (cf., Pik et al., 1998; Kempton et al., 2000;
70 Furman et al., 2006), and alternative models for LIP generation have been proposed (e.g.,

¹ We define as "fluid" a mobile phase which is not a carbonate or a silicate melt. Based on properties at the high P and T conditions of mantle rocks, fluids can have vapor-like, liquid-like, and transitional properties (cf., Manning, 2004; Keppler and Audéat, 2005)

71 Anderson, 2005; Foulger et al., 2005). The approach taken is a detailed study of H₂O bearing
72 phases (fluid inclusions, amphibole, and nominally anhydrous minerals) in a suite of amphibole-
73 bearing spinel lherzolites occurring at Injibara volcano, south-west of the Tana Lake (a summary of
74 the petrography, and major element mineral chemistry has been presented by Ferrando et al.,
75 2008). This volcanic centre is located on the Ethiopian plateau, at a marginal position with respect
76 to the Afar and the Main Ethiopian Rift, i.e *foci* of continental breakup.

77 We will bring the first direct evidence of chlorine-rich H₂O-CO₂ metasomatic fluids
78 preserved as inclusions in mantle minerals in the subcontinental lithosphere in a region of swelling
79 and flood basalt formation. The Cl-rich, C-O-H composition of the metasomatic fluid phase,
80 combined with calculated trace element patterns and H₂O-distribution in nominally anhydrous
81 minerals, allow us to trace fluid-rock interaction involved in lithospheric enrichment processes,
82 and to discuss fluid phase origin.

83

84 **2. GEOLOGICAL FRAMEWORK**

85

86 Ethiopia and Yemen have been affected by Oligocene to present flood basalt volcanism,
87 prior to and concomitantly with the formation of the Ethiopian Rift Valley and the Afar depression
88 (e.g., Mohr and Zanettin, 1988; Schilling and Kingsley, 1992; Deniel et al., 1994; Hofmann et al.,
89 1997). The abundant basaltic volcanism, forming a wide continental flood basalt province, was
90 accompanied by extensive regional uplift, and followed by rift opening and continental breakup
91 (e.g., Mohr and Zanettin, 1988). It built up a thick succession of tholeiitic to Na-alkaline lavas and
92 pyroclastic rocks, covering an area of about 600 km² (Fig. 1). Both the strong regional uplift
93 preceding or accompanying the magmatic activity, and the spatial distribution of magma types
94 have been interpreted by most Authors as evidence of emplacement of deep mantle plumes into
95 the lithosphere, generating continental breakup and extensive magmatic activity (e.g., Schilling,
96 1973; Hofmann et al., 1997; Pik et al., 1998, 1999; Ebinger and Casey, 2001; Kieffer et al., 2004).

97 Various stages of volcanic activity are recognized. The basaltic plateau was formed during
98 early stages, between about 50 to 10 Ma (e.g., Merla et al., 1979; Mohr and Zanettin, 1988), with
99 eruption of flood tholeiitic to transitional basalts; these were accompanied by eruption of mildly
100 alkaline trachytic and rhyolitic ignimbritic sheets, especially at the top of the basaltic sequence.
101 The bulk of basaltic magmas was erupted in a rather short time interval, around 30 ± 1 m.y.
102 (Zumbo et al., 1985; Baker et al., 1996; Hofmann et al., 1997; Ukstins et al., 2002). Successively,

103 several shield volcanoes of transitional to Na-alkaline basalts and minor trachytes were
104 constructed (e.g. Piccirillo et al., 1979). Finally, Pliocene to Present volcanic activity took place
105 mostly along the Main Ethiopian Rift and the Afar. Large variations in the petrological,
106 geochemical and volcanological characteristics of the volcanism have been observed both in space
107 and time in the Ethiopian-Afar-Red Sea volcanism (e.g., Deniel et al., 1994; Marty and Gezahegn,
108 1996; Pik et al., 1998, 1999; Chazot and Bertrand, 1993; Ayalew et al., 2002). These have been
109 interpreted as related either to heterogeneities within an ascending deep mantle plume (Pik et al.,
110 1999) and/or to interaction between deep plume material and the lithospheric mantle (Deniel et
111 al., 1994) with an important role of crustal contribution (Pik et al., 1999; Ayalew et al., 2002).

112 Most petrological data on the subcontinental lithospheric Ethiopian mantle were obtained
113 through the study of xenolith suites in Miocene-Quaternary alkali basalts from three different
114 sections (Fig. 1): the Northern Ethiopian Plateau (Lake Tana region: Conticelli et al., 1999; Roger et
115 al., 1999; Ferrando et al., 2008; Simien shield volcano: Ayalew et al., 2009), the Southern Main
116 Ethiopian Rift (Mega; Bedini et al., 1997; Conticelli et al., 1999), and the Central Main Ethiopian
117 Rift (Rooney et al., 2005). Beneath the Ethiopian plateau, Conticelli et al. (1999) and Roger et al.
118 (1999) described an heterogeneous lithosphere, consisting of spinel-lherzolites with very
119 subordinate harzburgites, dunites, and olivine websterites, which may locally contain amphibole.
120 Recently, in Quaternary basaltic lavas from a cinder cone located 7-8 km SW of Injibara (Lake
121 Tana region; Fig. 1), Ferrando et al. (2008) reported two suites of spinel-lherzolites: protogranular
122 to porphyroclastic Cl-pargasite-bearing spinel lherzolites ($T \leq 1000^\circ\text{C}$), which are also the subject of
123 the present study; and granular spinel lherzolites (\pm amphibole), which underwent thermal
124 recrystallization ($1043 - 1167^\circ\text{C}$). Geochemical studies allowed to propose that the lithosphere
125 beneath the Ethiopian plateau underwent two successive metasomatic events: modal
126 metasomatism induced by a hydrous metasomatic agent, followed by cryptic metasomatism by
127 alkali basaltic melts at higher temperatures.

128

129 **3. ANALYTICAL TECHNIQUES**

130

131 Major element analyses of minerals were carried out using a CAMECA SX50 electron
132 microprobe at the IGAG, CNR in Roma. Operating conditions were 15 kV accelerating voltage, 15
133 nA beam current, and 10 s counting time for element. Natural and synthetic standards include:
134 orthoclase (K), wollastonite (Ca, Si), native manganese (Mn), corundum (Al), jadeite (Na),

135 magnetite (Fe), native nickel (Ni), potassium chloride (Cl), periclase (Mg), native chromium (Cr),
136 and rutile (Ti). At the operating conditions, values below 0.05 wt% for minor elements must be
137 considered only indicative of very low contents (i.e. < 0.05 wt%). Structural formulae of minerals
138 were processed using the software of Ulmer (1986). For amphiboles, the nomenclature of Leake et
139 al. (2004) was followed.

140 In situ trace-element analysis of clinopyroxene and amphibole were performed on polished
141 petrographic thin sections (100 μm thick) using the Laser Ablation – Inductively Coupled Plasma –
142 Mass Spectrometer (LA-ICP-MS) installed at the University in Perugia (SMAArt facilities). The
143 instrumentation consists of a New Wave UP213 frequency quintupled Nd:YAG laser ablation
144 system coupled with a Thermo Electron X7 quadrupole based ICP-MS. All LA-ICP-MS
145 measurements were carried out using time resolved analysis operating in a peak jumping mode.
146 Each analysis consisted of ca. 40 s of measurement of instrumental background, i.e., analysis of
147 the carrier gas with no laser ablation, followed by ca. 60-80 s of data acquisition with the laser on.
148 The laser beam diameter, the repetition rate and the laser energy density were fixed to 30-40 μm ,
149 10Hz and $\sim 10\text{J}/\text{cm}^2$, respectively. Helium was preferred over argon as a carrier gas to enhance
150 transport efficiency of ablated aerosol (Eggins et al., 1998). The helium carrier exiting the ablation
151 cell was mixed with argon make-up gas before entering the ICP torch to maintain stable and
152 optimum excitation condition. External calibration was performed using NIST SRM 610 and 612
153 glass standards in conjunction with internal standardization using ^{42}Ca , previously determined by
154 electron microprobe WDS following the method proposed by Longerich et al. (1996). Data
155 reduction was performed using the Glitter software (van Achterbergh et al., 2001). The USGS
156 reference material BCR2G (a fused glass of the Columbia River Basalt) was analyzed in each
157 analytical run as quality control in order to assess the accuracy and the reproducibility of the
158 analyses. Precision and accuracy for trace element determination are better than 10% in the
159 standards. Further details on the analytical method can be found in Petrelli et al. (2007, 2008).

160 The composition of mineral phases within fluid inclusions was investigated with a
161 Cambridge Instruments SEM Stereoscan 360 equipped with an EDS Energy 200 and a Pentafet
162 detector (Oxford Instruments) at the University of Torino. Operating conditions were 15 kV
163 accelerating voltage and 50 s counting time. SEM-EDS quantitative data (spot size = 2 μm) were
164 acquired and processed using the Microanalysis Suite Issue 12, INCA Suite version 4.01; the raw
165 data were calibrated on natural mineral standards and the $\Phi\rho Z$ correction (Pouchou and Pichoir,
166 1988) was applied.

167 Microthermometric measurements in fluid inclusions were done in eight samples with a
168 Linkam THM 600 at the Siena University, calibrated using synthetic fluid-inclusion (SYNFLINC)
169 temperature standards. In the temperature interval between -90 and 40 °C, the accuracy was
170 estimated at 0.1°C at the standard reference points, and 0.2 °C at other temperatures. Isochores
171 for inclusions are calculated using the ISOC computer program (Bakker, 2003).

172 Raman spectra were acquired with a Labram microprobe (HORIBA, Jobin-Yvon), equipped
173 with a polarized 514.5-nm argon-ion laser at Siena University. The laser power was 300–500 mW
174 at the source and about 80% less at the sample surface. The slit width was 100 µm, and the
175 corresponding spectral resolution was $\pm 1.5 \text{ cm}^{-1}$. Raman spectra were collected through a 100×
176 Olympus objective (excitation spot 1–2 µm in size) for an acquisition time of 30 or 60 s.
177 Wavenumbers of the Raman lines were calibrated daily by the position of the diamond band at
178 $1,332 \text{ cm}^{-1}$. The assignment of the Raman peaks was done by comparison with the reference
179 database of mineral Raman spectra at the University of Siena
180 (http://www.dst.unisi.it/geofluids/raman/spectrum_frame.htm), if not otherwise indicated. The
181 analytical procedures applied for water detection in fluid inclusions are described in Frezzotti and
182 Peccerillo (2007).

183 Fourier transform infrared (FTIR) microspectroscopy was performed at the infrared beam-
184 line SISSI (Source for Imaging and Spectroscopic Studies in the Infrared) operating at the
185 synchrotron laboratory ELETTRA in Trieste. Spectra were collected on a FTIR spectrometer (Bruker
186 IFS66/v) fitted with an Hyperion IR microscopy with a liquid-nitrogen-cooled HgCdTe (MCT)
187 detector. Infrared microscopy was performed on a infrared microscopy system (Bruker) with a x 16
188 magnification infrared objective. Spectra were collected at resolution of 4 cm^{-1} and signal
189 averaged for 128 scans on each data collection. Background spectra were recorded in air. For IR
190 imaging studies, we used double-polished thick sections of xenoliths of known thickness. The
191 spectral images were collected scanning areas of variable sizes (200–400 µm-long and 200–400 µm-
192 wide), following a regular grid of square-aperture dimension of 20 µm equidistant by 20 µm in
193 both directions (i.e., totals of 100–400 spectra), using a computer-controlled automated X-Y
194 mapping stage.

195 Interpretation of unpolarized spectra of H₂O followed the classical group frequency
196 approach in which absorption bands are assigned to specific vibrational modes. OH concentrations
197 in mineral phases were estimated from the integrated absorbance using the Beer-Lambert law
198 (Paterson, 1982). Experimentally determined calibration constants for clinopyroxene and

199 orthopyroxene are from Bell et al. (1995), and for olivine are from Bell et al. (2003). Since
200 unpolarized FTIR H₂O measurements are affected by large errors (30-50 %; cf., Demouchy et al.,
201 2006), and imaging revealed H variations with position within single minerals, measuring the H₂O
202 amounts with a precision at the ppm scale was complicated; thus, measured water contents are
203 reported in intervals of tens of ppm, emphasizing the relative variations with distribution within
204 single grains.

205

206 **4. COMPOSITION OF PERIDOTITES**

207

208 Deformed spinel lherzolites have protogranular to porphyroclastic textures (Fig. 2a) and
209 contain two generations of olivine and orthopyroxene: large deformed porphyroclasts (2-4 mm),
210 and polygonal neoblasts (up to 1 mm). Exsolution lamellae of clinopyroxene are usually present
211 within porphyroclastic orthopyroxene (Fig. 2b). Clinopyroxene consists of smaller interstitial and
212 tabular grains (≈ 1 mm), containing spinel exsolution lamellae (Fig. 2c). Brownish spinel has
213 porphyroclastic or "holly-leaf" shape. Most deformed xenoliths contain weakly pleochroic
214 amphibole (0.5 – 1 mm). Amphibole usually occurs in contact with clinopyroxene, and always
215 contain relics of spinel, suggesting its grow from it (Fig. 2d).

216 Lherzolites have variable modal compositions with 50-69 olivine, 19-31 orthopyroxene, 9-
217 20 clinopyroxene, 2-7 spinel, and amphibole ≤ 1 , in vol.%. Comprehensive major element
218 compositions of minerals have been reported in Ferrando et al. (2008). Olivine has Mg-numbers
219 ($mg\# = Mg/(Mg+Fe_{tot}) * 100$) from 89.2 to 89.6, lower than average cratonic mantle (Pearson et al.,
220 2003). Spinel has $mg\#$ from 72.9 to 75.1, and $cr\#$ ($cr\# = Cr/(Cr+Al) * 100$) from 15 to 19 (Table 1).
221 Both porphyroclasts and neoblasts of orthopyroxene are enstatite, with $mg\# = 89.9-90.3$.

222 Clinopyroxene is a Ti-poor, Cr- Na-rich diopside ($mg\# = 89.8 - 91$; Table 1). Clinopyroxene
223 was analyzed for trace elements, illustrated in Fig. 3a and reported in Table 2. It shows LREE
224 enrichment relative to HREE [La 10 -15 PM; $(La/Yb)_N = 4 - 2.5$] and flat REE patterns. HREE are
225 relatively high, excluding re-equilibration with garnet, which would lead to much lower HREE
226 contents. Remarkable features are the positive anomalies in LILE, particularly Th, U, and Pb, (Pb_N
227 20), and the LILE/HFSE fractionation ($Pb_N/Nb_N = 10 - 50$). Ti, Zr, and Hf show modest negative
228 anomalies with respect to REE; Nb and Ta contents are lower than primordial mantle.

229 Amphibole is a Cr-rich pargasite, with $mg\# = 87.5-88.2$ (Table 1). Although mantle
230 amphibole is generally Cl-poor (typically < 0.05 wt %; e.g., Vannucci et al., 1995), pargasite has a

231 high Cl-content (0.33-0.37 wt%; Table 2). Pargasite has LREE [La 10 - 15 PM; (La/Yb)_N ≈ 4], Pb, U, Th,
232 and Sr enrichments quite similar to clinopyroxene (cf., Fig. 3 and Table 2), while tends to
233 concentrate Ba (Fig. 3b). Although amphibole is the main host for Nb and Ta (e.g. Ionov and
234 Hofmann, 1995), our pargasite does not show significant enrichments in these elements.

235

236 5. COMPOSITION AND DENSITY OF FLUID INCLUSIONS

237

238 Fluid inclusions are present in olivine and orthopyroxene porphyroclasts (Table 3; Fig. 4).
239 Clinopyroxene generally does not contain fluid inclusions, with exception of a few grains (Fig. 4).
240 Inclusions seem to have formed during a single fluid-rock interaction event; their distribution as
241 small clusters and along trails, which never reach grain boundary edges, is indicative for early
242 trapping (cf., Touret, 2001). Absence of inclusions in (olivine and orthopyroxene) neoblasts, in
243 pargasite, and in most clinopyroxene grains, indicate formation just prior to or contemporaneously
244 with recrystallization of peridotites. Glass (i.e., melt) has never been observed within fluid
245 inclusions, and melt inclusions and/or glass on grain boundaries are absent in peridotites.

246 In orthopyroxene porphyroclasts, fluid inclusions consist of CO₂ + H₂O, or CO₂ (CO₂ ≥ 80
247 vol. %; Fig. 4a and b). Liquid H₂O has been observed confined at the cavity borders only in a few
248 large irregularly-shaped inclusions (Table 3). Water within inclusions was further identified by
249 Raman analysis (Fig. 5a), and by microthermometric measurements (i.e., melting of clathrates, cf.
250 Table 3). In olivine porphyroclasts only a few among the inclusions contain CO₂ ± H₂O, while most
251 inclusions appear to have reacted with the host olivine, and are filled by aggregates of
252 phyllosilicates and a carbonate, without any noticeable fluid (step-daughter phases of Svensen et
253 al., 1999; Table 3; Fig. 4c and d). Raman analyses identify the association of talc, or clinocllore +
254 magnesite (Fig. 5b, c, and d). In clinopyroxene, rare fluid inclusions contain CO₂, but no H₂O or
255 solids, and form short alignments along with abundant tiny amphibole inclusions (20 - 80 μm;
256 arrows in Fig. 4e). Chemical analyses indicate these last ones as Cl-rich pargasite, identical to
257 pargasite in the host rock (Table 1). The absence of H₂O in fluid inclusions does not indicate that
258 the fluid was anhydrous: the association of Cl-pargasite + CO₂ inclusions testify for reaction of CO₂
259 - H₂O fluids with clinopyroxene to produce amphibole, leaving residual CO₂ trapped as inclusions.

260 CO₂ melting temperatures (T_{mCO₂}) were recorded between -57.6 and -56.2 °C (Table 3).
261 Despite this large scattering of temperatures, only in a few inclusions Raman analyses detected
262 traces of H₂S (< 0.1 mole %): the T_m's variation probably reflects thermal gradients within the

263 sample in the heating-cooling stage. A wide range of homogenization temperatures (T_h) to the
264 liquid phase was recorded between -39.2 and 31°C (Fig. 6). Water froze at temperatures of about
265 -50°C, and first melting (T_e) was recorded between -33 and -29°C (Table 3). Eutectic temperatures
266 are indicative for the presence of metals (e.g. Mg^{2+} and Fe^{2+}) in addition to Na^+ in the aqueous
267 fluid, and freezing above the $CaCl_2$ - $NaCl$ - H_2O eutectic at -52°C suggests little or no Ca^{2+} in solution.
268 In those inclusions containing both liquid and vapor CO_2 , clathrate melting temperatures ($T_{m,clat}$)
269 correspond to salinities of 14 - 10 wt. % in $NaCl$ eq. (Table 3).

270 The fluid composition was calculated as $X_{CO_2} = 0.64$, $X_{H_2O} = 0.33$, $X_{Na} = 0.006$, $X_{Mg} = 0.006$,
271 $X_{Cl} = 0.018$ (Bakker, 2003). In modeling fluid composition, Na^+ and Mg^{2+} ions in the aqueous part of
272 the fluid have been assumed present in subequal amounts, although the actual Mg/Na ratio of the
273 fluid is not known. Such an assumption does not affect the bulk fluid density, and only slightly
274 influences the Cl mole-fraction of the fluid. The resulting fluid density is 1.12 g/cm³. At the inferred
275 temperature of 950°C, based on mineral-mineral geothermometry (Ferrando et al., 2008), fluid
276 isochores correspond to minimum pressures of mantle equilibration between 1.4 and 1.5 GPa, or
277 50 - 54 km (Holloway, 1981).

278

279 **6. QUANTITATIVE H₂O MAPS IN NOMINALLY ANHYDROUS MINERALS**

280

281 Chemical mapping of H_2O distribution was performed in olivine and orthopyroxene
282 porphyroclasts and in clinopyroxene by synchrotron-sourced infrared microspectroscopy. The
283 study focused on: i) quantification and distribution of H_2O stored in nominally anhydrous minerals;
284 and ii) H_2O speciation and gradients between fluid inclusions and nominally anhydrous minerals.

285 In olivine not containing fluid inclusions, infrared absorption bands due to the stretching
286 vibration of OH bond were recorded between 3450 and 3600 cm⁻¹ (Fig. 7a and b). The wide
287 majority of spectra (about 100 – 150) per single investigated area reflects disturbance by
288 additional OH bands around 3680 cm⁻¹, which indicate the presence of talc and/or serpentine (Fig.
289 7c; Khisina et al., 2001; Matsyuk and Langer, 2004). Maps reveal that water is inhomogeneously
290 distributed at the 20x20 μm scale: from 40 ± 20 ppm up to more than 120 ppm, due to the
291 presence of hydrous phases (Fig. 7b). The image in Fig. 7c, reveals the distribution of
292 talc/serpentine as 20 - 40 μm inclusions, and possibly as lamellae at the nanometric scale (cf.
293 Khisina et al., 2001), since a general increase in the absorption intensities in the 3680 cm⁻¹ region
294 is observed through the analyzed area (yellow zone in Fig. 7c). In olivine containing fluid inclusions

295 exceedingly high water contents have been measured (200 - 440 ppm), which result from
296 additional extrinsic OH absorption bands from molecular water in inclusions, and from the
297 phyllosilicate formed by the reaction of the water contained within fluid inclusion and the host.

298 In inclusion-free clinopyroxene (Fig. 7d), water concentration ranges from 180 to 220 ppm,
299 and increases noticeably upon approaching the grain boundary (600 - 800 ppm). Water
300 enrichments are observed also within single crystals, where we document a an additional vibration
301 of water close to at 3670 cm^{-1} (Fig. 7f), which is attributed to structurally bound OH in small
302 nanometric pargasite inclusions (Hawthorne et al., 1997; Fig. 7e, and f). Rare clinopyroxene
303 containing fluid inclusions (Fig. 7g) shows similar OH gradients, with hydroxyl-enriched rims (20 -
304 $50\text{ }\mu\text{m}$) as illustrated in Fig. 7h. Chemical imaging in the $3600 - 3800\text{ cm}^{-1}$ region further shows that
305 hydration of clinopyroxene is coherent with the course of fluid inclusions (lower half of Fig. 7i).
306 Those areas surrounding inclusions, spectra (lower half of Fig. 7h) contain an additional vibration
307 at 3670 cm^{-1} , derived from extrinsic OH in pargasite inclusions (compare Fig. 7 h and i).

308 In orthopyroxene with no fluid inclusions, the chemical maps show a relatively
309 homogeneous water distribution, with contents in the range of 80 - 100 ppm. In orthopyroxene
310 containing fluid inclusions, a heterogeneous distribution of OH absorption intensities is observed,
311 systematically higher in fluid inclusion rich areas. Here, as much as 450 ppm H_2O have been
312 measured, due to additional absorption from extrinsic H_2O (molecular) contained in inclusions.
313 Further, mapping revealed positive water gradients moving towards the fluid inclusions: from 80
314 ppm, at about a $100\text{ }\mu\text{m}$ from the fluid inclusion trail, progressively increasing close to areas
315 containing inclusions (up to about 200 ppm; not shown). A similar gradient seem to indicate an
316 effective transition from molecular water into OH-bond, resulting from loss from inclusions
317 through dislocations and other defects (cf., Viti and Frezzotti, 2000).

318

319 **7. DISCUSSION**

320

321 **7.1 The peridotites**

322

323 Deformed spinel lherzolites represent a modally metasomatized lithosphere which
324 underwent progressive recrystallization at relatively low temperatures ($\leq 1000^\circ\text{C}$; Ferrando et al.,
325 2008). Isochores calculated from fluid inclusion density data locate their depth of origin at 1.4 and
326 1.5 GPa, or 50-55 km (Holloway, 1981; Bakker, 2003). The petrography and mineral chemistry of

327 peridotites indicate that metasomatism resulted during a single event, either by crystallization
328 from a melt or fluid phase, or by (melt-fluid)/solid reactions. Textural features, such as spinel being
329 replaced by pargasite (e.g., Fig. 2d), and presence of pargasite inclusion trails in clinopyroxene (Fig.
330 4f) are indicative of (melt-fluid)/rock reactions.

331 Inferences on the composition of the metasomatic agents can be derived from the trace
332 element composition of clinopyroxene and amphibole (Fig. 3). Clinopyroxene shows refertilization
333 as evidenced by selective enrichments in most incompatible elements (LREE, Pb, Sr, U, Th), marked
334 with depletion in HFSE. Amphibole mimics clinopyroxene trace element patterns, except for higher
335 Ba, Rb, Nb, Ta, Ti and Cl (Fig. 3). Partition coefficients for trace elements are consistent with the
336 clinopyroxene/amphibole relationships obtained from natural and experimental data (Ionov and
337 Hofmann, 1995; Tiepolo et al., 2001), and suggest equilibrium behavior.

338 The observed trace elements enrichments are consistent with equilibration of lherzolites
339 with an H₂O-rich metasomatic agent at high pressures: either an aqueous fluid, or a hydrous
340 silicate melt probably evolved through porous flow (Bedini et al., 1997; Zanetti et al., 1999; Laurora
341 et al., 2001; Ionov et al., 2002,; Rivalenti et al., 2004). Metasomatism mediated by carbonate-rich
342 melts seems unlikely, firstly because of the absence of geochemical unequivocal markers, such as
343 fractionation of Ti/Eu or Zr/Hf, and extreme LREE enrichment (up to 100 chondrite; Green and
344 Wallace, 1988; Yaxley et al., 1991; Rudnick et al., 1992; Yaxley and Green 1996). Further, at the
345 considered pressures, metasomatic carbonate melts would react with orthopyroxene to produce
346 clinopyroxene, converting lherzolite into wehrlite (e.g., Yaxley et al., 1991; Rudnick et al., 1993). The
347 investigated spinel lherzolites do not show any evidence for reaction of orthopyroxene, excluding
348 a similar scenario.

349 Based on trace element distribution in metasomatic minerals only, however, it is difficult to
350 discriminate between an aqueous fluid phase and a hydrous silica-rich melt as hypothetical
351 metasomatic agents. The absence of a substantial U/Th fractionation is different from what would
352 be expected from interaction with an aqueous fluid, but consistent with a silicate melt enriched in
353 water (Stalder et al., 1998). Conversely, both the Cl-, and Ba-rich composition of amphibole, and
354 the positive Pb/Sr correlation observed in amphibole and clinopyroxene suggests that the
355 observed incompatible element increase was mediated via an aqueous fluid phase, since all these
356 elements have high fluid/melt partition coefficients. The fractionation of Sr relative to Pb is also
357 consistent with equilibration with an aqueous fluid: Pb behaves significantly more incompatibly
358 than Sr in H₂O fluids: Pb and Sr are incorporated at similar rate only through partial melting

359 processes in silicate melts, or in supercritical fluids at higher pressures (cf., Brenan et al., 1994,
360 1995; Kessel et al., 2005).

361

362 **7.2. The metasomatic fluid phases**

363

364 To assess the nature of the metasomatic agents involved in mantle enrichment processes
365 in the Ethiopian lithospheric mantle, the chemical data from minerals are integrated with data
366 from fluid inclusions. Fluid inclusions indicate that rocks have interacted with a Cl-rich H₂O-CO₂
367 fluid, i.e. metasomatism was fluid mediated. Further, the high Cl-content in pargasite, and the
368 common association of fluid inclusions with pargasite inclusions in clinopyroxene suggests that Cl-
369 rich fluids were contemporaneous and parental to pargasite growth.

370 Fluids contained within inclusions are dominated by CO₂ (≥ 64 mol.%). This corresponds to
371 a_{H₂O} of 0.2 of the fluid phase at the considered pressures. However, the original water content is
372 underestimated, as infrared maps show H₂O diffusion from the inclusions to the host phase. The
373 aqueous part of the fluid contain Cl, Na, and Mg - but not Ca - with salinities ranging between 10
374 and 14 % in NaCl + MgCl₂ eq. wt. (2 molal [NaCl - MgCl₂] solution). The Cl content is high, and
375 calculated between 4 - 5 in mole %, depending on the Mg/Na ratio. Cl-rich fluids should also have
376 contained SiO₂ and Al₂O₃, as suggested by formation of clinocllore and talc in inclusions reacting
377 with olivine host (Pawley, 2003). At mantle conditions, high solubility of Si and Al is predicted, due
378 to polymerization of these solutes in aqueous solutions, although the presence of CO₂ and NaCl
379 tends to counteract this process (Newton and Manning, 2000).

380 Aqueous fluids involved in mantle enrichment processes at high pressure (1-2 GPa),
381 especially concentrated solutions, have different properties than pure H₂O fluids; high Cl-contents
382 (> 1 molal %) are known to strongly increase the solubility of metals (Mg, Fe, and Pb) and LILE
383 (Keppler, 1996; Green and Adam, 2003; Manning, 2004). To better understand the possible effects
384 of a high chlorine activity, trace element compositions of model fluids in equilibrium with
385 clinopyroxene have been calculated, using experimental partition coefficients for clinopyroxene-
386 H₂O (D_{cpx-H₂O}), and for clinopyroxene-H₂O 5 molal NaCl (D_{cpx-brine}) (Keppler, 1996; Ayers, 1998); the
387 results are shown in Fig. 8a. Calculated patterns for model brines (5 molal NaCl in Fig. 8a) in
388 equilibrium with clinopyroxene show increasing higher incompatible element abundance,
389 associated with prominent Pb and Sr positive anomalies and negative HFSE anomalies. Conversely,
390 D_{cpx-H₂O}, yields model pure H₂O fluids with relatively unfractionated patterns, undepleted in HFSE,

391 and with significant enrichments only in Pb and U (H₂O in Fig. 8a). Model brines in equilibrium with
392 clinopyroxene approach the composition of slab-derived brines (Fig. 8b; Scambelluri et al., 2002),
393 and, to a lesser extent, that of carbonate-brine fluids in diamonds of eclogites (Fig. 8b; Tomlinson
394 et al., 2009), but not that of carbonate-brine fluid in kimberlites (Fig. 8b; Tomlinson et al., 2009).

395 Thus, the metasomatic enrichment in the lithosphere beneath the Ethiopian plateau could
396 have been induced by Cl-rich fluids preserved in fluid inclusions. Model trace-element composition
397 appears to suggest similarities with patterns of slab-derived Cl-rich aqueous fluids. This last
398 observation, however, should be taken cautiously, since geochemical inconsistencies with deep
399 brines in diamonds could result from differences in fluid composition (i.e., presence of a carbonate
400 component), and properties at different pressures.

401

402 **7.3. Fluid distribution and content in the Ethiopian lithosphere**

403

404 In the African lithospheric mantle, metasomatic growth of amphibole driven by hydrous
405 “fluids” is observed in several localities and supposed to have occurred during the early stages of
406 mantle upwelling. The amphibole-rich mantle under the Chyulu Hill Volcanic Province of southern
407 Kenya is considered to have been modally metasomatized during early stages of the plume rising
408 in the East African Rift (Späth et al., 2001). In a similar way, the growth of amphibole ± apatite in
409 spinel peridotites from Yemen, is considered to have occurred during or shortly after the
410 Oligocene by the influx of carbonatitic melts and hydrous fluids from the Afar plume (Baker et al.,
411 1998). Besides, Cl-rich pargasite in spinel lherzolites of Zabargad Island (Red Sea) is interpreted to
412 have grown just before the early rifting phase of the Red Sea (Agrinier et al., 1993). Metasomatism
413 in spinel lherzolite suite demonstrates a major role for aqueous fluids also in the lithosphere
414 beneath the Ethiopian plateau.

415 Minor pargasite in lherzolites is generally considered to be indicative of reaction of mantle
416 rocks with minor amounts of hydrous fluids or melts. Present study argues for the presence of
417 significant amounts of Cl-rich C-O-H- fluids in the Ethiopian lithosphere, which have a low water
418 activity, resulting from presence of chlorine and other dilutants (e.g., CO₂). In addition to
419 amphibole, water was stored into olivine and pyroxenes. Minimum calculated water contents
420 within these nominally anhydrous minerals range around 40 ± 20 ppm for olivine, 100 ± 20 for
421 orthopyroxene, and 220 ± 20 for clinopyroxene, corresponding to minimum water content of
422 deformed lherzolites ≤ 150 ppm. These values are consistent with water contents measured in

423 nominally anhydrous minerals in spinel lherzolites (e.g., Ingrin and Skogby, 2000), and with
424 equilibrium partitioning of water between olivine and pyroxenes at the considered pressures
425 (Ingrin and Skogby, 2000; Bell and Rossman, 1992, Hauri et al., 2004).

426 Microinfrared maps of water distribution, however, identify zones of water enrichments at
427 the scale of the individual grain, generally not readily available, when measuring water with single
428 spot analyses: i) in most samples, olivine shows incipient hydration and locally stores up to 200 -
429 400 ppm H₂O (e.g. micro- to nano-inclusions of mg-phyllsilicates; Fig. 7b. ii). In clinopyroxene,
430 H₂O contents show a gradient, with extreme enrichments (up to 700 - 800 ppm) in the last 50 μm
431 at grain boundaries, and along intragranular bands in the internal parts (Fig. 7e, and h). Such a
432 zoning does not correspond to any other element (major or trace) zoning, with exception of a
433 slight La enrichment (Fig. 3); it could be considered suggestive of the presence of growth defects,
434 probably resulting from recrystallization in presence of aqueous fluids.

435 These observations lead to the conclusion that locally water amounts within deformed
436 spinel lherzolites could have been significantly higher and up to 400 - 500 ppm, without any
437 increase of the amount of amphibole in the rocks. Such an inhomogeneous water enrichment
438 through lherzolites has profound effects on the physical and chemical properties of lithospheric
439 mantle rocks: a heterogeneous distribution of those trace elements which are transported by
440 aqueous fluids, and a local overstep of C-O-H peridotite solidus, inducing partial melting, without
441 significant increases of temperatures.

442

443 **7.4. Significance of Cl-rich fluids in a region of asthenosphere upwelling and flood basalts.**

444

445 At Hawaii and Azores oceanic settings, Cl-enrichment in the lithosphere is indicated by the
446 high Cl/F ratios of melt inclusions in OIB, and interpreted to reflect shallow interaction with sea-
447 water or with deep-crustal brines (e.g., Michael and Schilling, 1989; Seaman et al., 2004; Stolper et
448 al., 2004; Le Roux et al., 2006). A similar explanation cannot apply to the continental lithospheric
449 mantle beneath the Ethiopian plateau. Here, metasomatism implies fluxes of C-O-H metasomatic
450 fluid phases rich in Cl and incompatible elements into the lithospheric mantle, likely related to
451 upwelling of the Afar mantle zone. Interactions between metasomatic fluids and mantle rocks
452 seem to have occurred heterogeneously, most likely by fracture migration, inducing selective
453 enrichments in volatiles and incompatible elements (LILE, and LREE) in the lithosphere. The source

454 of metasomatic fluids should have been located either in the upwelling asthenospheric mantle, or
455 in the lithosphere, where they started to migrate under the effect of increasing thermal anomalies.

456 Present data rise the question of Cl-enrichment in mantle fluids within the context of the
457 geodynamic evolution of the East African region. The high water and chlorine content (4-5 mole %)
458 of fluids suggests the presence of a cycled crustal (i.e., altered oceanic lithosphere) component in
459 their source. This is agreement with the extreme enrichments in Pb, Ba, Th, U, and Sr preserved in
460 amphibole and clinopyroxene, as generally assumed for sediments entrained in subducting
461 lithosphere (e.g. Ben Othman et al., 1989). Recycling of carbon has been shown in carbonatite
462 melts in oceanic peridotite xenoliths (e.g. Hauri et al., 1993) and can occur also for Cl, as Cl-rich
463 fluids found in eclogites and serpentinites can be recycled into the convecting mantle (cf., Pyle and
464 Mather, 2009, and references therein).

465 The upper mantle beneath Ethiopia was affected by ancient (Pan-African) subduction
466 processes. Therefore, it can be hypothesized that these elemental enrichments may be a remnant
467 of ancient subduction processes that were preserved in a fossilized lithospheric-asthenospheric
468 mantle, until the emplacement of hot mantle material generated their mobilization by
469 dehydration-decarbonation reactions, forming an ascending metasomatic Cl-rich CO₂-H₂O fluid
470 front. According to this hypothesis, the asthenospheric contribution to magmatism in the plateau
471 would be a function of both time (early magmatism more affected by lithosphere; Vidal et al.,
472 1991) and position with respect to Afar, which is the focus of extensional processes generated by
473 uprise of deep mantle material (Corti, 2009).

474 The preservation of textures, mineralogy, and fluid inclusions in a fossilized mantle for
475 hundreds of Ma after the Pan African orogeny is, however, enigmatic. An alternative scenario is
476 that CO₂ - brine fluids were derived by decarbonation and outgassing of deep hydro-saline
477 carbonate melts at pressures below 2 - 2.5 GPa. Presence of chlorine- and carbonate-rich fluid
478 phases at depth in the mantle would be consistent with the composition and metasomatic
479 signature of fluid phases preserved in diamonds at pressures above 4-5 GPa (Izraeli et al., 2001;
480 Klein-BenDavid et al., 2004; 2007; Tomlinson et al., 2009), and with melts in kimberlites
481 (Kamenetsky et al., 2004, 2007). Carbonate melts might have been generated by low degrees of
482 melting of a carbonated fertile peridotite, or of a carbonated and hydrated eclogite (Dalton and
483 Presnal 1988; Gudfinnsson and Presnall, 2005; Dasgupta and Hirschmann, 2006; Dasgupta et al.,
484 2007). Such melts have very low viscosities, and can rise through the upper mantle, degassing a
485 CO₂-H₂O-Cl fluid phase at pressures below the carbonate-stability field (2-2.5 GPa; Dobson et al.,

486 1996; Hammouda and Laporte, 2003). Noteworthy, fluxing of metasomatic CO₂ and H₂O from
487 outgassing of hydrous carbonate melts has been recently proposed in the lithosphere beneath
488 Hawaii, based on the association of CO₂-H₂O fluids, carbonates, and diamonds preserved in fluid
489 inclusions of garnet pyroxenite xenoliths (Frezzotti and Peccerillo, 2007).

490

491 8. Summary

492

493 In conclusion, present data provide the first direct evidence for Cl-rich CO₂-H₂O fluids
494 fluxing the lithosphere of a region of continental flood basalts. Despite the uncertainties in the
495 fluid recycling record, the chemical and physical properties of Cl-rich fluids suggest an origin in the
496 upper mantle, probably at pressure above 2.5 GPa. Volatile enrichment and refertilization in the
497 lithosphere beneath the Ethiopian plateau induced by Cl-rich fluids might have played a key role in
498 facilitating melting, such that magmatism could have been generated without a significant
499 increase of mantle temperatures. Further, elemental enrichment by similar fluids may provide an
500 explanation for the geochemical trace element signature of some LIP magmas (i.e., strong positive
501 spikes of Ba and Pb). Finally, our findings complement ongoing fluid inclusion research in
502 diamonds and kimberlites (e.g., Izraeli et al., 2001; Kamenetsky et al., 2004; 2007; Klein-BenDavid
503 et al., 2004; 2007; Tomlinson et al., 2009) and highlight the important role of Cl in aqueous fluids
504 at mantle depth.

505

506 **ACKNOWLEDGEMENTS**

507

508 We are grateful for the constructive reviews from M. A. Menzies and three anonymous
509 reviewers. We are indebted to M. Serracino for assistance during microprobe analyses. This work
510 was funded by national (MIUR 2008) funds to M.L.F. and A.P.. Raman analyses facilities were
511 provided by PNRA, the national research group for Antarctica. Access to the Synchrotron in Trieste
512 was funded by Elettra and the EU.

513

514 REFERENCES

- 515 Agrinier P., Mével C., Bosch D., and Javoy M. (1993) Metasomatic hydrous fluids in amphibole
516 peridotites from Zabargad Island (Red Sea). *Earth Planet. Sci. Lett.* **120**, 187-205.
- 517 Andersen T. and Neumann E. R. (2001) Fluid inclusions in mantle xenoliths. *Lithos* **55**, 301-320.
- 518 Anderson D. L. (2005) Large igneous provinces, delamination, and fertile mantle. *Elements* **1**, 271-
519 275.
- 520 Ayalew D., Barbey P., Marty B., Reisberg L., Yirgu G. and Pik R. (2002) Source, genesis, and timing
521 of giant ignimbrite deposits associated with Ethiopian continental flood basalts. *Geochim.*
522 *Cosmochim. Acta* **66**, 1429-1448.
- 523 Ayalew D., Arndt N., Bastien F., Yirgu G., and Kiefer B. (2009) A new mantle xenolith locality from
524 Simien shield volcano, NW Ethiopia. *Geol. Mag.* **146**, 144-149.
- 525 Ayers J. (1998) Trace element modeling of aqueous fluid– peridotite interaction in the mantle
526 wedge of subduction zones. *Contrib. Mineral. Petrol.* **132**, 390-404.
- 527 Baker J. A. , Snee L. and Menzies M. (1996) A brief Oligocene period of flood volcanism in Yemen:
528 implications for the duration and rate of continental flood volcanism at the Afro-Arabian
529 triple junction. *Earth Planet. Sci. Lett.* **138**, 39-55.
- 530 Baker J. A., Chazot C., Menzies M., and Thirwall M. (1998) Metasomatism of the shallow mantle
531 beneath Yemen by the Afar plume: Implications for plumes, flood volcanism, and intraplate
532 volcanism. *Geology* **26**, 431-434.
- 533 Bakker R. J. (2003) Package FLUIDS 1. New computer programs for the analysis of fluid inclusion
534 data and for modelling bulk fluid properties. *Chem. Geol.* **194**, 3-23.
- 535 Bedini R. M., Bodinier J. L., Dautria J. M. and Morten L. (1997) Evolution of LILE-enriched small
536 melt fractions in the lithospheric mantle: a case study from the East African Rift. *Earth Planet.*
537 *Sci. Lett.* **153**, 67-83.
- 538 Bell D. R. and Rossman G. R. (1992) Water in Earth's mantle: The role of nominally anhydrous
539 minerals. *Science* **255**, 1391-1397.
- 540 Bell D. R., Ihinger P. D., and Rossman G. R. (1995) Quantitative analysis of trace OH in garnet and
541 pyroxenes. *Am. Mineral.* **80**, 465-474.
- 542 Bell D. R., Rossman G. R., Maldener J., Endisch D., and Rauch F. (2003) Hydroxide in olivine: a
543 quantitative determination of the absolute amount and calibration of the IR spectrum. *J.*
544 *Geophys. Res.* **108**, 2105. doi:10.1029/2001JB000679
- 545 Ben Othman D., White W. M., and Patchett J. (1989) The geochemistry of marine sediments, island
546 arc magma genesis, and crustal-mantle recycling. *Earth Planet. Sci. Lett.* **94**, 1-21.
- 547 Brenan J. M., Shaw H. F., Phinney D. L., and Ryerson F. J. (1994) Rutile-aqueous fluid partitioning of
548 Nb, Ta, Hf, Zr, U and Th: implications for high field strength element depletions in island-arc
549 basalts. *Earth Planet. Sci. Lett.* **128**, 327-339.
- 550 Brenan J. M., Shaw H. F., Ryerson F. J., and Phinney D. L. (1995) Mineral-aqueous fluid partitioning
551 of trace elements at 900°C and 2.0 GPa: Constraints on the trace chemistry of mantle and
552 deep crustal fluids. *Geochim. Cosmochim. Acta* **59**, 3331-3350.
- 553 Chazot G. and Bertrand H. (1993) Mantle sources and magma-continental crust interactions during
554 early Red Sea-Aden rifting in Southern Yemen: Elemental and Sr, Nd, Pb isotope evidence. *J.*
555 *Geophys. Res.* **98**, 1818-1835.
- 556 Condie K.C. (2001) Mantle Plumes and Their Records in Earth History, pp. 306. Cambridge
557 University Press, New York.
- 558 Corti G. (2009) Continental rift evolution: From rift initiation to incipient break-up in the Main
559 Ethiopian Rift, East Africa. *Earth Sci. Rev.* **96**, 1-53.

560 Conticelli S., Sintoni M. F., Abebe T., Mazzarini F., and Manetti P. (1999) Petrology and
561 geochemistry of ultramafic xenoliths and host lavas from the Ethiopian Volcanic Province: an
562 insight into the upper mantle under Eastern Africa. *Acta Vulcanol.* **11**, 143-159.

563 Dalton J. A. and Presnall D. C. (1998) The continuum of primary carbonatitic–kimberlitic melt
564 compositions in equilibrium with lherzolite: Data from the system CaO-MgO-Al₂O₃-SiO₂-CO₂
565 at 6 GPa. *J. Petrol.* **39**, 1953-1964.

566 Dasgupta R. and Hirschmann M. M. (2006) Melting in the Earth's deep upper mantle caused by
567 carbon dioxide. *Nature* **440**, 659-662.

568 Dasgupta R., Hirschmann M. M., and Smith N. D. (2007). Partial melting experiments of peridotite
569 + CO₂ at 3 GPa and genesis of alkalic ocean island basalts. *J. Petrol.* **48**, 2093-2124.

570 Demouchy S., Jacobsen S. D., Gaillard F., and Stern C. R. (2006) Rapid magma ascent recorded by
571 water diffusion profiles in mantle olivine. *Geology* **34**, 429-432.

572 Deniel C., Vidal P., Coulon C., Vellutini P. J., and Pigué P. (1994) Temporal evolution of mantle
573 sources through continental rifting: The volcanism of Djibouti (Afar). *J. Geophys. Res.* **99**,
574 2853-2869.

575 Dobson, D.P., Jones A.P., Rabe R., Sekine T., Kurita K., Taniguchi T., Kondo T., Kato T., Shimomura
576 O., and Urakawa S. (1996) In-situ measurement of viscosity and density of carbonate melts at
577 high pressure. *Earth Planet. Sci. Lett.* **143**, 207-215.

578 Ebinger C. J. and Casey M. (2001) Continental breakup in magmatic provinces: An Ethiopian
579 example. *Geology* **29**, 527-530.

580 Eggins S.M., Kinsley L. P. J., and Shelley J. M. G. (1998) Deposition and fractionation processes
581 during atmospheric pressure laser sampling for analysis by ICP-MS. *Appl. Surf. Sci.* **129**, 278.

582 Ernst R. E. Buchan K. L. (2003) Recognizing mantle plumes in the geological record. *Annual Rev.*
583 *Earth Planet. Sci.* **31**, 469-523.

584 Falloon T. J. and Green D. H. (1989) The solidus of carbonated, fertile peridotite. *Earth Planet. Sci.*
585 *Lett.* **94**, 364-370.

586 Ferrando S., Frezzotti M. L., Neumann E. R., De Astis G., Peccerillo A., Dereje A., Gezahegn Y., and
587 Teklewold A. (2008) Composition and thermal structure of the lithosphere beneath the
588 Ethiopian plateau: evidence from mantle xenoliths in basanites, Injibara, Lake Tana Province.
589 *Mineral. Petrol.* **93**, 47-78.

590 Foulger G. R., Natland J. H., Presnall D. C., and Anderson D. L. (Eds.) (2005) Plates, Plumes and
591 Paradigms, pp. 881. Special Publication **388**. Geological Society of America.

592 Frezzotti M. L. and Peccerillo A. (2007) Diamond-bearing COHS fluids in the mantle beneath Hawaii.
593 *Earth Planet. Sci. Lett.* **262**, 273-283.

594 Frezzotti M. L., Andersen T., Neumann E. R., and Simonsen S. L. (2002a) Carbonatite melt-CO₂ fluid
595 inclusions in mantle xenoliths from Tenerife, Canary Islands: a story of trapping, immiscibility
596 and fluid–rock interaction in the upper mantle. *Lithos* **64**, 77-96.

597 Frezzotti M. L., Neumann E. R., and Touret J. L. R. (2002b) Ephemeral carbonate melts in the upper
598 mantle: carbonate-silicate immiscibility in microveins and inclusions within spinel peridotite
599 xenoliths, La Gomera, Canary Islands. *Eur. J. Mineral.* **14**, 5, 891-904.

600 Frost R., Palmer S., Bouzaid J. and Reddy J. (2007) A Raman spectroscopic study of humite minerals.
601 *J. Raman Spectr.* **38**, 68-77.

602 Furman T., Bryce J., Rooney T., Hanan B., Yirgu G., and Ayalew D. (2006) Heads or tails: 30 million
603 years of the Afar plume. In *The structure and Evolution of the east African rift system in the*
604 *Afar volcanic province* (eds. G. Yirgu, C. J. Ebinger, and P.K.H. Maguire) pp. 97-121. Special
605 Publication **259**. Geological Society of London.

606 Green D. H. and Wallace M. E. (1988) Mantle metasomatism by ephemeral carbonatite melts.
607 *Nature* **336**, 459-462.

- 608 Green D. H. and Falloon T. J. (1998) Pyrolite: a Ringwood concept and its current expression. In *The*
609 *Earth's Mantle* (ed. J. Jackson), Cambridge Univ. Press, New York, pp. 311-378.
- 610 Green T. H. and Adam J. (2003) Experimentally-determined trace element characteristics of
611 aqueous fluid from partially dehydrated mafic oceanic crust at 3.0 GPa, 650-700°C. *Eur. J.*
612 *Mineral.* **15**, 815-830.
- 613 Gudfinnsson G.H. and Presnall D.C. (2005) Continuous gradations among primary carbonatitic,
614 kimberlitic, melilititic, basaltic, picritic, and komatiitic melts in equilibrium with garnet
615 lherzolite at 3-8 GPa. *J. Petrol.* **46**, 1645-1659.
- 616 Hammouda T. and Laporte D. (2000) Ultrafast mantle impregnation by carbonatite melts. *Geology*
617 **28**, 283-285.
- 618 Hauri E.H., Shimizu N., Dieu, J.J., and Hart S.R. (1993) Evidence for or hotspot-related carbonatite
619 metasomatism in the oceanic upper mantle. *Nature* **365**, 221-227.
- 620 Hauri E. H., Gaetani G., and Green T. H. (2004) Partitioning of H₂O between mantle minerals and
621 silicate melts, *Geochim. Cosmochim. Acta* **68**, A33 (abstr.).
- 622 Hawthorne F. C., Della Ventura G., Robert J.-L., Welch M. D., Raudsepp M., and Jenkins D. M.
623 (1997) A Rietveld and infrared study of synthetic amphiboles along the potassium-rich-tremolite-
624 tremolite join. *Am. Mineral.* **82**, 708-716.
- 625 Hofmann C., Courtillot G., Feraud G., Rochette P., Yirgu G., Ketefo E., and Pik R. (1997) Timing of
626 the Ethiopian flood basalt event and implication for plume birth and global change. *Nature*
627 **389**, 838-841.
- 628 Holloway J.R. (1981) Compositions and volumes of supercritical fluids in the earth's crust. In *Short*
629 *course in fluid inclusions: Applications to petrology* (eds. L.S. Hollister and M.L. Crawford)
630 Mineral. Ass. Canada, Calgary, pp. 13-38.
- 631 Ingrin J. and Skogby H. (2000) Hydrogen in nominally anhydrous upper-mantle minerals:
632 Concentration levels and implications. *Eur. J. Mineral.* **12**, 543-570.
- 633 Ionov D. A. and Hofmann A. W. (1995) Nb-Ta-rich mantle amphiboles and micas: implications for
634 subduction-related metasomatic trace element fractionations. *Earth Planet. Sci. Lett.* **131**,
635 341-356.
- 636 Ionov D. A., Bodinier J.-L., Mukasa S. B., and Zanetti A. (2002) Mechanisms and sources of mantle
637 metasomatism: major and trace element compositions of peridotite xenoliths from
638 Spitsbergen in the context of numerical modeling. *J. Petrol.* **43**, 2219-2259.
- 639 Izraeli E. S., Harris J. W., and Navon O. (2001) Brine inclusions in diamonds: a new upper mantle
640 fluid. *Earth Planet. Sci. Lett.* **187**, 323-332.
- 641 Kamenetsky M.B., Sobolev A.V., Kamenetsky V.S., Maas R., Danyushevsky L.V., Thomas R.,
642 Pokhilenko N.P., Sobolev N.V. (2004). Kimberlite melts rich in alkali chlorides and
643 carbonates: a potent metasomatic agent in the mantle. *Geology* **32**, 845-848.
- 644 Kamenetsky V.S., Kamenetsky M.B., Sharygin V.V., Faure K., Golovin A.V. (2007) Chloride and
645 carbonate immiscible liquids at the closure of the kimberlite magma evolution (Udachnaya-
646 East kimberlite, Siberia). *Chem. Geol.* **237**, 384-400.
- 647 Kempton P.D., Fitton J.G., Saunders A.D., Nowell G.M., Taylor R.N., Hardarson B.S., and Pearson G.
648 (2000) The Iceland plume in space and time. *Earth Planet. Sci. Lett.* **177**, 255-271.
- 649 Keppler H. (1996) Constraints from partitioning experiments on the composition of subduction-
650 zone fluids. *Nature* **380**, 237-240.
- 651 Keppler H. and Audétat A. (2005) Fluid-mineral interaction at high pressures. In *Mineral behavior*
652 *at extreme conditions* (ed. R. Miletich), Eur. Mineral. Union, Lecture notes in Mineral. **7**. pp.
653 1-30.
- 654 Kessel R., Schmidt M. W., Ulmer P., and Pettke T. (2005) Trace element signature of subduction-
655 zone fluids, melts and supercritical liquids at 120-180 km depth. *Nature* **437**, 724-727.

656 Khisina N. R., Wirth R., Andrut M., and Ukhanov A.V. (2001) Extrinsic and intrinsic mode of
657 hydrogen occurrence in natural olivines: FTIR and TEM investigation. *Phys. Chem. Miner.* **28**,
658 291-301.

659 Kieffer B., Arndt N., Lapierre H., Bastien F., Bosch D., Pecher A., Yirgu G., Ayalew D., Weis D.,
660 Jerram D. A., Keller F., and Meugniot C. (2004) Flood and shield basalts from Ethiopia:
661 magmas from the African Superswell. *J. Petrol.* **45**, 793-834.

662 Klein-BenDavid O., Izraeli E. S., Hauri E., and Navon O. (2004) Mantle fluid evolution—a tale of one
663 diamond. *Lithos* **77**, 243-253.

664 Klein-BenDavid O., Izraeli E. S., Hauri E., and Navon O. (2007) Fluid inclusions in diamonds from the
665 Diavik mine, Canada and the evolution of diamond-forming fluids. *Geochim. Cosmochim.*
666 *Acta* **71**, 723-744.

667 Kleppe A. K., Jephcoat A. P., and Welch M. D. (2003) The effect of pressure upon hydrogen
668 bonding in chlorite: A Raman spectroscopic study of clinocllore to 26.5 GPa. *Am. Mineral.* **88**,
669 567-573.

670 Laurora A., Mazzucchelli M., Rivalenti G., Vannucci R., Zanetti A., Barbieri M. A., and Cingolani C. A.
671 (2001) Metasomatism and Melting in Carbonated Peridotite Xenoliths from the Mantle
672 Wedge: The Gobernador Gregores Case (Southern Patagonia). *J. Petrol.* **42**, 69-87.

673 Le Roux P. J., Shirey S. B., Hauri E. H., Perfit M. R., and Bender J. F. (2006) The effects of variable
674 sources, processes and contaminants on the composition of northern EPR MORB (8-108N
675 and 12-148N): Evidence from volatiles (H₂O, CO₂, S) and halogens (F, Cl). *Earth Planet. Sci.*
676 *Lett.* **251**, 209-231.

677 Leake B. E., Woolley A. R., Birch W. D., Burke E. A. J., Ferraris G., Grice J. D., Hawthorne F. C., Kisch
678 H. J., Krivovichev V. G., Schumacher J. C., Stephenson N. C. N., and Whittaker E. J. W. (2004)
679 Nomenclature of amphiboles: additions and revisions to the International Mineralogical
680 Association's amphibole nomenclature. *Eur. J. Mineral.* **16**, 191-196.

681 Longerich H. P., Jackson S. E., and Günter D. (1996) Laser ablation-inductively coupled plasma mass
682 spectrometric transient signal data acquisition and analyte concentration calculation. *J. Anal.*
683 *Atomic Spectrom.* **11**, 899-904.

684 Manning C. E. (2004) The chemistry of subduction-zone fluids. *Earth Planet. Sci. Lett.* **223**, 1-16.

685 Marty B., Pik R., and Gezahegn Y. (1996) Helium isotopic variations in Ethiopian plume lavas:
686 Nature of magmatic sources and limit on lower mantle contribution. *Earth Planet. Sci. Lett.*
687 **144**, 223-237.

688 Matsyuk S. S. and Langer K. (2004) Hydroxyl in olivines from mantle xenoliths in kimberlites of the
689 Siberian Platform. *Contrib. Mineral. Petrol.* **147**, 413-437.

690 McDonough W. F. and Sun S. S. (1995) Composition of the earth. *Chem. Geol.* **120**, 223-253.

691 Merla G., Abbate E., Canuti P., Sagri M., and Tacconi P. (1979) Geological map of Ethiopia and
692 Somalia and comment, pp. 89. Consiglio Nazionale delle Ricerche, Firenze.

693 Michael, P. J. and Schilling J.-G. (1989) Chlorine in mid-ocean ridge magmas: evidence for
694 assimilation of seawater-influenced components. *Geochem. Cosmochim. Acta* **53**, 3131-3143.

695 Mohr P. and Zanettin B. (1988) The Ethiopian flood basalt province. In *Continental Flood Basalts*
696 (ed. J. D. Macdougall), pp. 63-110. Kluwer Academic Publishing.

697 Navon O., Hutcheon I. D., Rossman G. R., and Wasserburg G. J. (1988) Mantle-derived fluids in
698 diamond micro-inclusions. *Nature* **335**, 784-789.

699 Newton R.C. and Manning C.E. (2000) Quartz solubility in concentrated aqueous NaCl solutions at
700 deep crust– upper mantle metamorphic conditions: 2-15 kbar and 500-900 °C. *Geochim.*
701 *Cosmochim. Acta* **64**, 2993– 3005.

702 Paterson M. (1982) The determination of hydroxyl by infrared absorption in quartz, silicate glasses
703 and similar materials: *Bull. Minéral.* **105**, 20-29.

704 Pawley A. (2003) Chlorite stability in mantle peridotite: the reaction clinocllore + enstatite =
705 forsterite + pyrope + H₂O. *Contrib. Mineral. Petrol.* **144**, 449-456.

706 Petrelli M., Perugini D., Poli G., and Peccerillo A. (2007) Graphite electrode tetraborate fusion for
707 automated trace element determination in bulk samples by laser ablation ICP-MS. *Microchim.*
708 *Acta* **158**, 275-282.

709 Petrelli M., Perugini D., Alagna K. E., Poli G., and Peccerillo A. (2008) Spatially Resolved and Bulk
710 Trace Element Analysis by Laser Ablation - Inductively Coupled Plasma - Mass Spectrometry
711 (LA-ICP-MS). *Per. Mineral.* **77**, 3-21.

712 Piccirillo E. M., Justin-Visentin E., Zanettin B., Joron J. K., and Treuil M. (1979) Geodynamic
713 evolution from plateau to rift: Major and trace element geochemistry of the central eastern
714 Ethiopian plateau volcanics. *Neues Jahr. Geol. Palaont.* **258**, 139-179.

715 Pik R., Deniel C., Coulon C., Yirgu G., Hofmann C., and Ayalew D. (1998) The Northwestern
716 Ethiopian plateau flood basalts: Classification and spatial distribution of magma types. *J.*
717 *Volcanol. Geotherm. Res.* **81**, 91-111.

718 Pik R., Deniel C., Coulon C., Yirgu G., and Marty B. (1999) Isotopic and trace element signatures of
719 Ethiopian flood basalts: Evidence for plume-lithosphere interaction. *Geochim. Cosmochim.*
720 *Acta* **63**, 2263-2279.

721 Pouchou J. L. and Pichoir F. (1988) Determination of mass absorption coefficients for soft X-Rays
722 by use of the electron microprobe. In *Microbeam Analysis*, pp. 319–324. San Francisco Press.

723 Pyle D. M. and Mather T. A. (2009) Halogens in igneous systems. *Chem. Geol.* **263**, 110-121.

724 Rivalenti G., Mazzucchelli M., Laurora A., Ciuffi S. I. A. , Zanetti A., Vannucci R., and Cingolani C. A.
725 (2004) The backarc mantle lithosphere in Patagonia, South America. *J. South Am. Earth Sci.*
726 **17**, 121-152.

727 Roedder E. (1965) Liquid CO₂ inclusions in olivine-bearing nodules and phenocrysts from basalts
728 *Am. Mineral.* **50**, 1746-1782.

729 Roger S., Dautria J. M., Coulon C., Pik R., Yirgu G., Michard A., Legros P., and Ayalew D. (1999) An
730 insight on the nature, composition and evolution of the lithospheric mantle beneath in the
731 north-western Ethiopian plateau: the ultrabasic xenoliths from the Tana Lake Province. *Acta*
732 *Vulcanol.* **11**, 161-168.

733 Rooney T. O., Furman T., Yirgu G., and Ayalew D. (2005) Structure of the Ethiopian lithosphere:
734 xenolith evidence in the Main Ethiopian Rift. *Geochim. Cosmochim. Acta* **69**, 3889-3910.

735 Rudnick R. L., McDonough W. F., and Orpin A. (1992) Tanzanian peridotite xenoliths: a comparison
736 with Kaapvaal peridotites and inferences on metasomatic interactions. In *Kimberlites, related*
737 *rocks and mantle xenoliths*. Vol. 1. (eds. H. O. A. Meyer and O. Leonardos) pp. 336-353. Proc.
738 5th Inter. Kimberlite Conf., CPRM, Brasilia.

739 Rudnick R. L., McDonough W. F., and Chappell B. W. (1993) Carbonatite metasomatism in the
740 Northern Tanzanian mantle - petrographic and geochemical characteristics. *Earth Planet. Sci.*
741 *Lett.* **114**, 463-475.

742 Scambelluri M., Bottazzi P., Trommsdorff V., Vannucci R., Hermann J., Gomez-Pugnaire M.T.,
743 Lopez-Sanchez Vizcaino V. (2002) Incompatible element-rich fluids released by antigorite
744 breakdown in deeply subducted mantle, *Earth Planet. Sci. Lett.*, **192**, 457–470.

745 Schiano P., Clocchiatti R., Shimizu N., Maury R. C., Jochum K. P., and Hoffman A.W. (1995) Hydrous
746 silica-rich melts in the sub-arc mantle and their relationship with erupted arc lavas. *Nature*
747 **377**, 595-600.

748 Schilling J. G. (1973) Afar mantle plume: Rare earth evidence. *Nature* **242**, 2-5.

749 Schilling J.G. and Kingsley R.H. (1992) Nd–Sr–Pb isotopic variations along the Gulf of Aden:
750 evidence for Afar Mantle Plume – Continental Lithosphere interaction. *J Geophys. Res.* **97**
751 (B7): 10927–10966

752 Seaman C., Sherman S. B., Garcia M. O., Baker M. B., Balta B., and Stolper E. (2004) Volatiles in
753 glasses from the HSDP2 drill core. *Geochem. Geophys. Geosyst.* **5**, Q09G16 doi:
754 10.1029/2003GC000596

755 Späth A., Le Roex A. P., and Opiyo-Akech N. (2001) Plume-lithosphere interaction and the origin of
756 continental rift-related alkali volcanism-the Chyulu Hills volcanic province, southern Kenya. *J.*
757 *Petrol.* **42**, 765-787.

758 Stalder R., Foley S. F., Brey G. P., and Horn I. (1998) Mineral-aqueous fluid partitioning of trace
759 elements at 900-1200°C and 3.0-5.7 GPa: new experimental data for garnet, clinopyroxene,
760 and rutile, and implications for mantle metasomatism - evidence from high-pressure
761 experiments and natural rocks. *Geochim. Cosmoch. Acta* **62**, 1781-1801.

762 Stolper E., Sherman S., Garcia M. O., Baker M. B., and Seaman C. (2003) Glass in the submarine
763 section of the HSDP2 drill core, Hilo, Hawaii. *Geochem. Geophys. Geosyst.* **5**, Q07G15, doi:
764 10.1029/2003GC000553.

765 Svensen H., Jamtveit B., Yardley B. W., Eengvik A. K., Austrheim H. and Broman C. (1999) Lead and
766 Bromine enrichment in eclogite facies fluids: extreme fractionation during lower crustal
767 hydration. *Geology* **27**, 467-470.

768 Thompson A. B. (1992) Water in the Earth's Upper Mantle. *Nature* **358**, 295-302.

769 Tiepolo M., Bottazzi P., Foley S., Oberti R., Vannucci R., and Zanetti A. (2001) Fractionation of Nb
770 and Ta from Zr and Hf at mantle depths: the role of titanian pargasite and kaersutite. *J. Petrol.*
771 **42**, 221-232.

772 Tomlinson E.L., Müller W. and EIMF (2009) A snapshot of mantle metasomatism: Trace element
773 analysis of coexisting fluid (LA-ICP-MS) and silicate (SIMS) inclusions in fibrous diamonds.
774 *Earth Planet. Sci. Lett.* **279**, 362-372.

775 Touret J.L.R. (2001) Fluids in metamorphic rocks. In *Fluid inclusions: Phase relationships – methods*
776 *– applications*. (eds. T. Andersen, M.L. Frezzotti, E. Burke), pp. 1-27. *Lithos* **55**.

777 Ukstins I., Rennes P., Wolfenden E., Baker J., Ayalew D., and Menzies M. (2002) Matching
778 conjugate volcanic rifted margins: $^{40}\text{Ar}/^{39}\text{Ar}$ chronostratigraphy of pre- and syn-rift bimodal
779 flood volcanism in Ethiopia and Yemen. *Earth Planet. Sci. Lett.* **198**, 289-306.

780 Ulmer P. (1986) NORM-Program for cation and oxygen mineral norms. Computer Library, Institut
781 für Mineralogie und Petrographie, ETH-Zentrum, Zürich, Switzerland.

782 van Achterbergh E., Ryan C. G., Jackson S., and Griffin W. L. (2001) Data reduction software for LA-
783 ICP-MS. In *Laser-Ablation-ICPMS in the earth sciences, principles and applications* (ed. P.
784 Sylvester), pp. 239-243. Short Course Series **29**. Mineralogical Association Canada.

785 Vannucci R., Piccardo G. B., Rivalenti G., Zanetti A., Rampone E., Ottolini L., Oberti R., Mazzucchelli
786 M., and Bottazzi P. (1995) Origin of LREE-depleted amphiboles in the subcontinental mantle.
787 *Geochim. Cosmochim. Acta* **59**, 1763-1771

788 Vidal P. H., Deniel C., Vellutini P. J., Pigué P., Coulon C., Vincent J., and Audin J. (1991) Changes of
789 mantle sources in the course of a rift evolution: The Afar case. *Geophys. Res. Lett.* **18**, 1913-
790 1916.

791 Viti C. and Frezzotti M.L. (2000) Re-equilibration of glass and CO₂ inclusions in xenolith olivine: a
792 TEM study. *Am. Mineral.* **85**, 1390-1396.

793 Wallace M. E. and Green D. H. (1988) An experimental-determination of primary carbonatite
794 magma composition. *Nature* **335**, 343-346.

795 White R. S. and McKenzie D. (1995) Mantle plume and flood basalts. *J. Geophys. Res.* **100**, 17543-
796 17585.

797 Wyllie P. J. and Ryabchikov I. D. (2000) Volatile components, magmas, and critical fluids in
798 upwelling mantle. *J. Petrol.* **41**, 1195-1206.

799 Yaxley G. M., Crawford A. J., and Green, D. H. (1991) Evidence for alkaline glasses and carbonatite
800 metasomatism in spinel peridotite xenoliths from western Victoria, Australia. *Earth Planet.*
801 *Sci. Lett.* **107**, 305–317.
802 Yaxley G. M. and Green D. H. (1996) Experimental reconstruction of sodic dolomitic carbonatite
803 melts from metasomatised lithosphere. *Contrib. Mineral. Petrol.* **124**, 359-369.
804 Zanetti A., Mazzucchelli M., Rivalenti G., and Vannucci R. (1999) The Finero phlogopite-peridotite
805 massif: an example of subduction-related metasomatism. *Contrib. Mineral. Petrol.* **134**, 107-
806 122.
807 Zumbo V., Feraud G., Bertrand H., and Chazot G (1995) $^{40}\text{Ar}/^{39}\text{Ar}$ chronology of Tertiary magmatic
808 activity in southern Yemen during the early Red Sea-Aden rifting. *J. Volcanol. Geother. Res.*
809 **65**, 265-279.
810
811

812 **Figure captions**
813

814 Fig. 1. Simplified geological sketch map of Ethiopia, reporting sampling locality (black star)
815 modified from Conticelli et al., 1999, Roger et al., 1999, and Kieffer et al., 2004. MER: Main
816 Ethiopian Rift; EVP: Ethiopian Volcanic Plateau.

817 Fig. 2. Photomicrographs of spinel lherzolites from Injibara. a) Deformed lherzolite showing
818 porphyroclastic texture. Sample INJ35, crossed polars (CP). b) Porphyroclast of orthopyroxene
819 showing exsolution lamellae of clinopyroxene. Sample INJ16, plane-polarized light (PPL). c)
820 Clinopyroxene in textural equilibrium with porphyroclastic olivine. Spinel segregations are
821 evident within clinopyroxene. Sample INJ16, PPL. d) Relict “holly-leaf” Spl partly replaced by
822 brown-to-yellow amphibole. A very fine-grained corona grows on it. Sample INJ35, PPL. Ol I =
823 olivine porphyroclast; Ol II = olivine neoblast; Opx II orthopyroxene neoblast; Cpx =
824 clinopyroxene; Spl = spinel.

825 Fig. 3. Trace element concentrations (a) in clinopyroxene (Cpx) core and rim, and (b) in amphibole,
826 normalized to primordial mantle (PM) using the data from McDonough and Sun (1995). Data
827 below detection limits that connected with dashed lines and plotted as detection limit values.

828 Fig. 4. Photomicrographs of fluid inclusions in spinel lherzolites. a) Fluid inclusion distribution
829 along microfractures in orthopyroxene. A few large inclusions (arrow) still contain CO₂ (liquid +
830 vapor) and liquid H₂O at the cavity rim (see Raman spectrum in Fig. 5a). Sample INJ 34 (PPL). b)
831 Decrepitated CO₂ fluid inclusion trails within orthopyroxene. Large decrepitation aoes surround
832 single or groups of fluid inclusions (arrow). Sample INJ 7 PPL. c) Trail of CO₂ fluid inclusions in
833 olivine. Most inclusions appear dark and consist of talc/clinochlore + magnesite, having CO₂ and
834 H₂O reacted with olivine host. Around reacted inclusions, large yellowish aoes are present
835 (arrow). Sample INJ 34 PPL. d) Preserved CO₂ ± H₂O inclusions in olivine. Inclusions are
836 disposed along a transposed trail. Sample INJ 16 PPL. e) CO₂ fluid inclusions in clinopyroxene.
837 Amphibole inclusions of similar size are observed (arrow). Sample INJ 1. PPL. f) Back scattered
838 electron image showing fluid inclusion (black) and amphibole (dark gray) distribution in
839 clinopyroxene. Spinel inclusions and segregations are also visible (white). Sample INJ 16.

840 Fig. 5. Raman spectra of (a) H₂O in fluid inclusions in orthopyroxene, and of (b) clinochlore
841 (hydroxyls), (c) talc (hydroxyls), and (d) magnesite in reacted fluid inclusions in olivine.
842 Clinochlore hydroxyl vibrations at 3450, 3638, 3673 cm⁻¹, from Kleppe et al., 2003; the
843 additional vibration at 3565 cm⁻¹ might be indicative for excess of Al, or for the additional

844 presence of humite (Frost et al., 2007). In spectrum d, non assigned peaks correspond to host
845 olivine.

846 Fig. 6. Histogram of homogenization temperatures to the liquid phase (T_h) recorded in fluid
847 inclusions. Homogenization temperature intervals up to 50 °C were often registered within a
848 single inclusion trail. n = number of measurements.

849 Fig. 7. Synchrotron infrared imaging of water distribution in olivine and clinopyroxene from
850 deformed lherzolites. Each set of maps includes a microscopic image in plane polarized light,
851 and relative infrared maps in selected absorbance regions. *a-b-c*: a) investigated area in one
852 olivine grain. PPL. b) Absorbance map in the 3000 - 3600 cm^{-1} region and calculated water
853 contents in olivine (ppm). c) Qualitative distribution map of OH absorbance for clinocllore, talc,
854 and serpentine in the 3600 - 3800 cm^{-1} region , which allows to qualify hydrated phases in
855 olivine. *d-e-f*: d) Clinopyroxene not containing fluid inclusions. PPL. e) Absorbance map in the
856 3000 - 3800 cm^{-1} region and relative calculated water contents in clinopyroxene (ppm). f)
857 Qualitative OH absorbance map in the 3600 - 3800 cm^{-1} region relative to distribution of
858 amphibole inclusions. *g-h-i*: g) Clinopyroxene containing a trail of fluid inclusions. PPL. h)
859 Absorbance map in the 3000 - 3800 cm^{-1} region and relative calculated water contents in
860 clinopyroxene (ppm). i) Qualitative OH absorbance distribution map in the 3600 - 3800 cm^{-1}
861 region relative to distribution of amphibole inclusions. Sizes of investigated areas are in micron.
862 Measured water contents are drawn with a precision of 10's of ppm (see text). a.u. = arbitrary
863 units.

864 Fig. 8. Trace element composition of model aqueous fluids in equilibrium with clinopyroxene of
865 Injibara lherzolites. The trace element concentrations are normalized to primordial mantle (PM)
866 using the data from McDonough and Sun (1995). a) Trace element composition of model
867 aqueous fluids (pure H_2O , and brines - 5 molal NaCl solution) in equilibrium with clinopyroxene,
868 based on experimental partition coefficient data (Keppler, 1996; Ayers, 1998). b) Comparison of
869 model brine composition with trace element patters measured in Cl-rich fluid inclusions formed
870 at mantle depth; compositional range of slab-derived brines generated by antigorite
871 breakdown, from Scambelluri et al., 2002; carbonate-brine fluids in diamonds from peridotites
872 and eclogites, from Tomlinson et al., 2009.

873

Table 1

Representative chemical analyses of olivine, orthopyroxene and spinel

Sample	INJ16	INJ16	INJ16	INJ16	INJ16	INJ37	INJ4	INJ7	INJ16	INJ16	INJ35	INJ35	INJ4	INJ7	INJ16	INJ16		
Mineral	OI I	OI II	Opx I av	Opx II av	Spl	Spl	Cpx core	Cpx core	Cpx rim	Cpx rim	Cpx core	Cpx core	Pargasite	Pargasite	Amp FI	Amp FI		
Analyses	14ol39	23ol81	inj16opxC	inj16opxB	9spl8	72spl49	i4cpx49	i7cpx20	i16cpx15	i16cpx17	i35cpx12r	i35cpx64	i4amp24	i7amp22	21Amp136	21Amp139		
	2 analyses		2 analyses														EDS	EDS
SiO ₂ wt%	40.94	40.91	55.67	55.8	0.07	0.04	52.6	52.76	52.51	52.21	52.41	52.62	42.81	42.97	42.1	41.97		
TiO ₂	< 0.01	< 0.01	0.11	0.11	0.2	0.14	0.47	0.56	0.53	0.58	0.45	0.54	2.54	2.46	2.45	2.73		
Cr ₂ O ₃	0.02	0.01	0.41	0.36	16.78	14.35	1.02	0.81	0.92	0.93	0.99	0.85	1.27	1.53	1.55	1.66		
Al ₂ O ₃	0.03	0.01	3.51	3.65	51.17	52.69	5.69	5.4	5.55	5.47	5.65	5.67	14.17	14.35	14.26	14.19		
Fe ₂ O ₃	0	0	0.53	0.76	2.16	2.21	0.88	0.37	0	0.1	0	0	4.88	4.63	4.56	4.36		
FeO	10.52	10.2	6.02	5.75	10.83	9.63	1.97	2.74	2.78	2.77	3.08	3.03	0	0	0.35	0.35		
MnO	0.12	0.17	0.16	0.15	<0.01	<0.01	0.05	0.07	0.04	0.03	0.02	0.14	< 0.01	< 0.01	< 0.10	< 0.10		
MgO	48.79	49.14	33.23	33.51	19.25	19.7	15.65	15.54	15.12	15.37	15.18	15.06	17.21	17.5	17.33	17.31		
NiO	0.51	0.31	0.06	0.12	0.32	0.4	0.03	0.07	0.06	< 0.01	0.03	0.01	0.1	0.2	< 0.10	< 0.10		
CaO	0.05	0.02	0.62	0.59	< 0.01	0.01	20.48	20.27	20.11	20.24	20.27	20.17	10.4	10.44	11.34	11.15		
Na ₂ O	< 0.02	< 0.02	0.09	0.06	< 0.02	< 0.02	1.54	1.52	1.46	1.46	1.45	1.52	3.99	4	3.7	3.82		
K ₂ O	0.01	0.01	0.01	0.01	0.01	< 0.01	< 0.01	< 0.01	0.01	0.02	0.01	< 0.01	0.07	0.1	< 0.10	< 0.10		
Cl	-	-	-	-	-	-	-	-	-	-	-	-	0.34	0.37	0.37	0.32		
H ₂ O	-	-	-	-	-	-	-	-	-	-	-	-	2.03	2.04	2.11	2.11		
Total	100.99	100.78	100.39	100.91	100.78	99.17	100.38	100.11	99.09	99.18	99.54	99.61	99.81	100.6	100.09	100.02		
Cl=O													0.08	0.08	0.08	0.07		
Total													99.73	100.51	100.02	99.94		
Si a.p.f.u.	1	1	1.92	1.91	0	0	1.89	1.91	1.92	1.9	1.91	1.91	6.06	6.03	5.98	5.97		
Al ^{IV}	-	-	0.08	0.09	1.59	1.65	0.11	0.09	0.08	0.1	0.09	0.09	1.94	1.97	2.02	2.03		
Al ^{VI}	-	-	0.06	0.06	-	-	0.14	0.14	0.16	0.14	0.15	0.16	0.42	0.4	0.37	0.35		
Ti	-	-	0	0	0	0	0.01	0.02	0.01	0.02	0.01	0.01	0.27	0.26	0.26	0.29		
Cr	0	0	0.01	0.01	0.35	0.3	0.03	0.02	0.03	0.03	0.03	0.02	0.14	0.17	0.17	0.19		
Fe ³⁺	0	0	0.01	0.02	0.04	0.04	0.02	0.01	-	-	-	-	0.52	0.49	0.49	0.47		
Fe ²⁺	0.21	0.21	0.17	0.16	0.24	0.21	0.06	0.08	0.08	0.08	0.09	0.09	-	-	0.04	0.04		
Mn	0	0	0	0	-	-	-	-	-	-	-	-	-	-	-	-		
Mg	1.77	1.78	1.71	1.71	0.76	0.78	0.84	0.84	0.82	0.84	0.82	0.82	3.63	3.66	3.67	3.67		
Ni	0.01	0.01	0	0	0.01	0.01	0	0	0		0	0	0.01	0.02	-	-		
Ca	0	0	0.02	0.02	-	0	0.79	0.78	0.79	0.79	0.79	0.79	1.58	1.57	1.73	1.7		
Na	-	-	0.01	0	-	-	0.11	0.11	0.1	0.1	0.1	0.11	1.1	1.09	1.02	1.05		
K	0	0	0	0	0	-	-	-	0	0	0	-	0.01	0.02	-	-		
Cl	-	-	-	-	-	-	-	-	-	-	-	-	0.08	0.09	0.09	0.08		
OH	-	-	-	-	-	-	-	-	-	-	-	-	1.92	1.91	2	2		
mg#	89.2	89.6	90.1	90.3	72.9	75.1	91	90	90.6	90.5	89.8	89.9	87.5	88.2	87.4	87.8		
cr#	-	-	-	-	18	15												

EDS analyses of the tiny amphibole grains associated to fluid inclusions (Amp FI) are reported for comparison. OI I = porphyroclast; OI II = neoblasts; Opx I = porphyroclast; Opx II = neoblast; Spl = spinel. mg# = Mg/(Mg+Fetot)*100; cr# (cr# = Cr/Cr+Al*100)

Table 2

Representative trace element analyses in clinopyroxene (Cpx) and amphibole (Amp)

Sample	INJ4	INJ7	INJ16	INJ16	INJ35	INJ35	INJ4	INJ7
Mineral	Cpx core	Cpx core	Cpx rim	Cpx rim	Cpx core	Cpx core	Pargasite	Pargasite
Analyses	i4cpx49	i7cpx20	i16cpx15	i16cpx17	i35cpx12r	i35cpx64	i4amp24	i7amp22
ppm								
Sc	82	62	95	105	74	73	44	42
V	250	261	243	245	230	238	354	378
Cr	-	-	-	-	-	-	8574	9361
Co	21.7	21.5	18.6	18.6	19.5	20	43.4	44.4
Ga	4	3	3	3	3	4	7	6
Rb	< 0.1	< 0.1	< 0.1	< 0.1	< 0.1	< 0.1	1.3	1.11
Sr	148	151	168	175	158	145	388	423
Y	17	12	21	22	20	19	19	16
Zr	38	25	43	47	40	41	31	26
Nb	< 0.1	0.5	< 0.1	< 0.1	< 0.1	< 0.1	8	10.7
Cs1	< 0.1	< 0.1	< 0.1	< 0.1	< 0.1	< 0.1	< 0.1	< 0.1
Ba	<0.4	13	<0.4	<0.4	<0.4	2	285	356
La	7.3	6.8	9.6	9	7.5	7.3	8.3	8.3
Ce	10	12	12	12	10	9	13	15
Pr	1.2	1.3	1.6	1.6	1.1	1.1	1.4	1.6
Nd	6	6	8	8	7	6	7	7
Sm	1.9	1.6	2.6	2.7	2.1	2.1	2.2	1.9
Eu	0.65	0.64	0.91	0.95	0.99	0.83	0.93	0.79
Gd	2.4	2.2	2.9	3.1	3.3	3.2	3.2	2.7
Tb	0.39	0.29	0.56	0.48	0.52	0.47	0.51	0.44
Dy	3.5	2.5	4.2	3.7	3.4	3.6	3.5	3
Ho	0.63	0.47	0.86	0.77	0.75	0.79	0.78	0.56
Er	2.2	1.5	2.5	2.5	2.2	2.3	2	1.7
Tm	0.3	0.19	0.29	0.37	0.26	0.33	0.32	0.27
Yb	2	1.3	2.2	2.2	1.8	2	1.7	1.6
Lu	0.29	0.19	0.29	0.33	0.22	0.29	0.29	0.21
Hf	1.2	0.7	1.2	1.3	1.5	1.3	0.7	0.7
Ta	0.03	0.04	< 0.009	0.04	< 0.009	< 0.009	0.3	0.53
Pb	2.3	2.8	1.9	1.9	2.1	3.1	9	10.5
Th	0.75	0.56	0.89	0.93	0.78	0.74	0.69	0.67
U	0.18	0.17	0.16	0.18	0.19	0.18	0.19	0.23
K	< 83	< 83	83	166	83	< 83	582	831
Ti	2818	3357	3177	3477	2698	3237	15227	14748

Table 3
Summary fluid inclusion properties

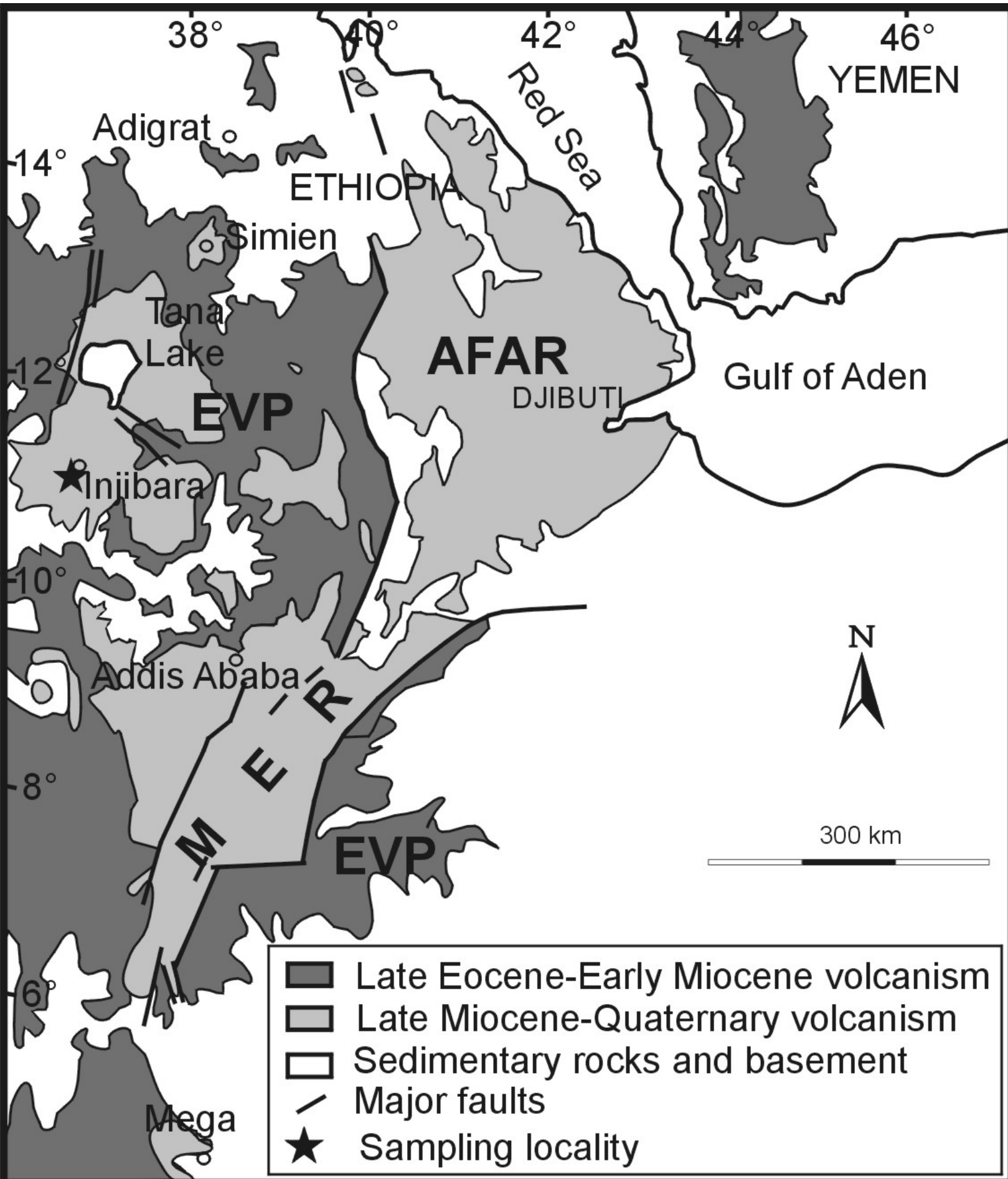
Petrography

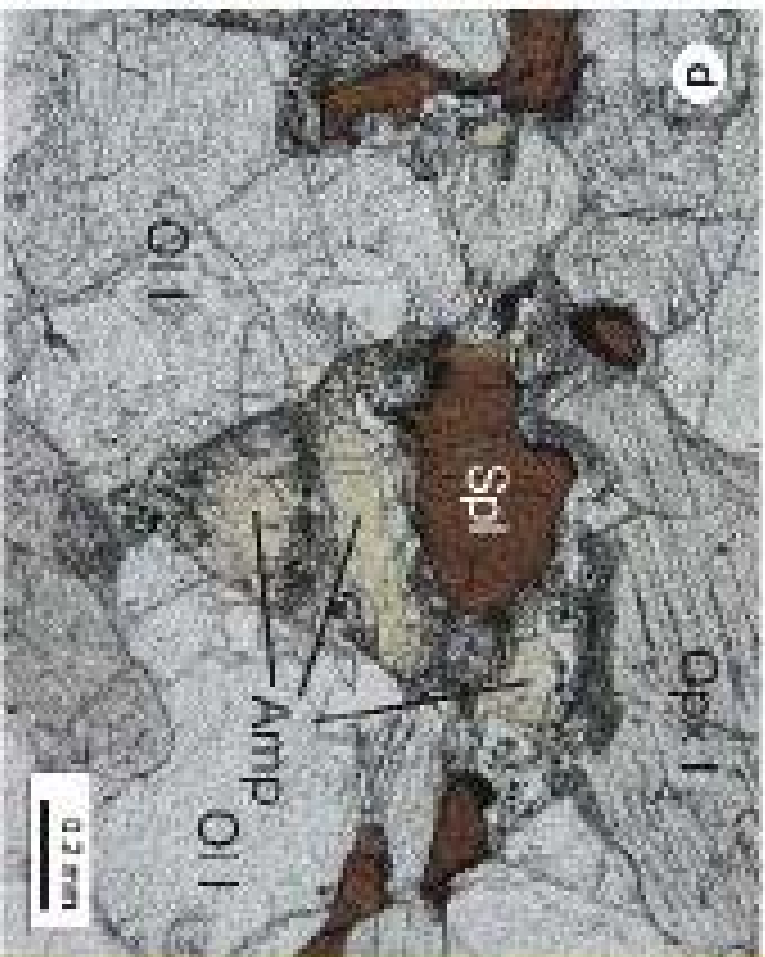
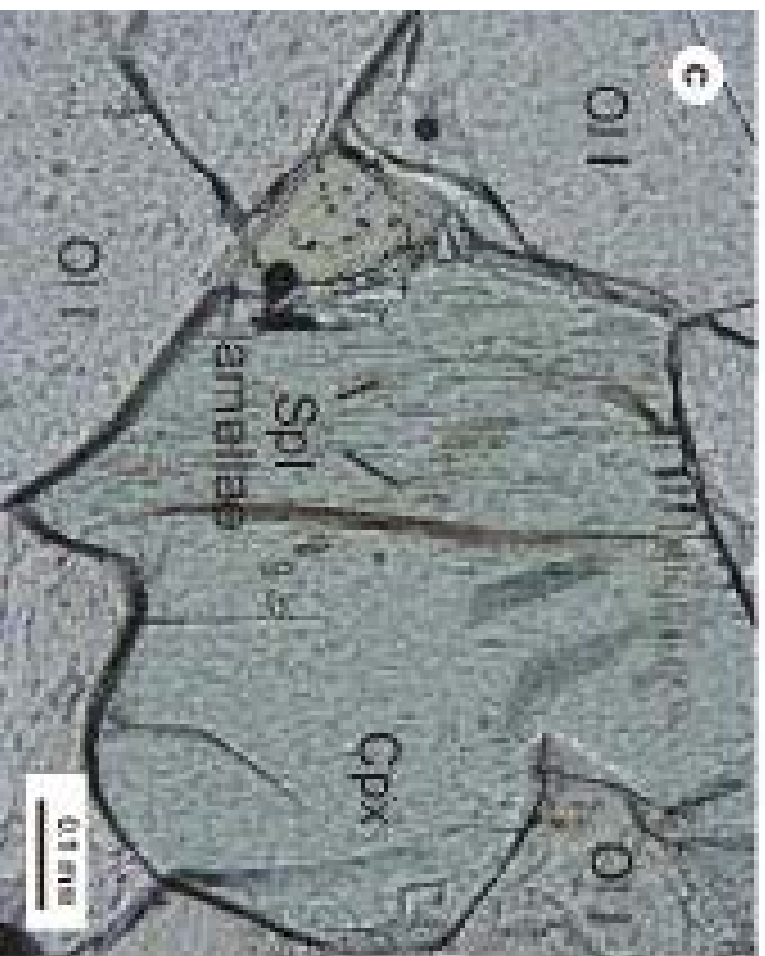
Host phase	Composition		Textural characteristics			liquid H ₂ O detection			
	Preserved	Reacted	Size (µm)	Distribution	Abundance	Optical	Microtherm.	Raman	IR
OI I	CO ₂ H ₂ O	± Mg-chlorite (Talc) + Magnesite	<3 - 30	early in porphyroclasts	present in most grains	no	yes	yes	yes
Opx I	CO ₂ H ₂ O	± no	<3 - 60	early in porphyroclasts	present in most grains	yes	yes	yes	yes
Cpx	CO ₂	-	<3 - 30	early with amphibole	rare	no	no	no	no

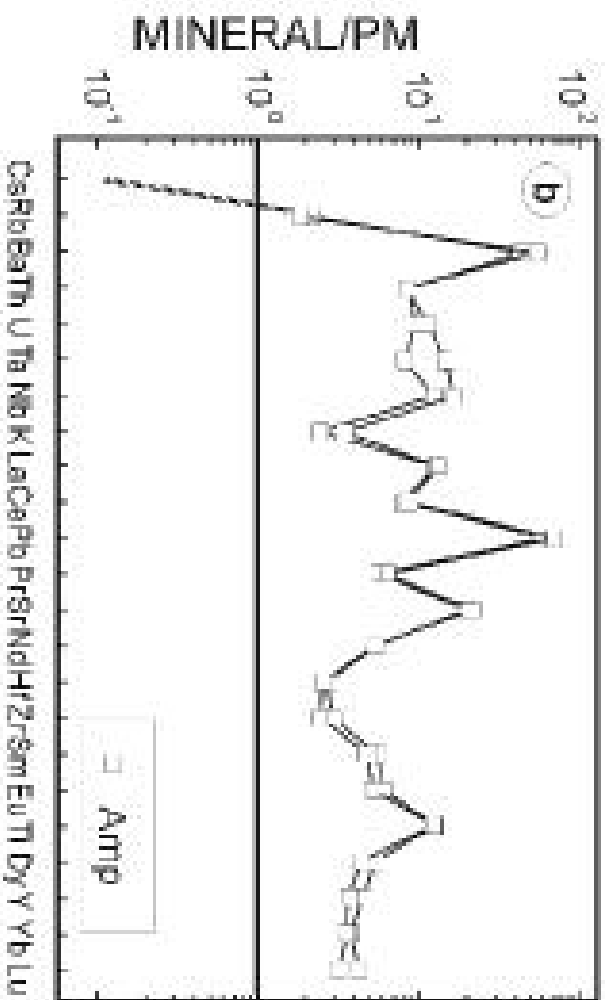
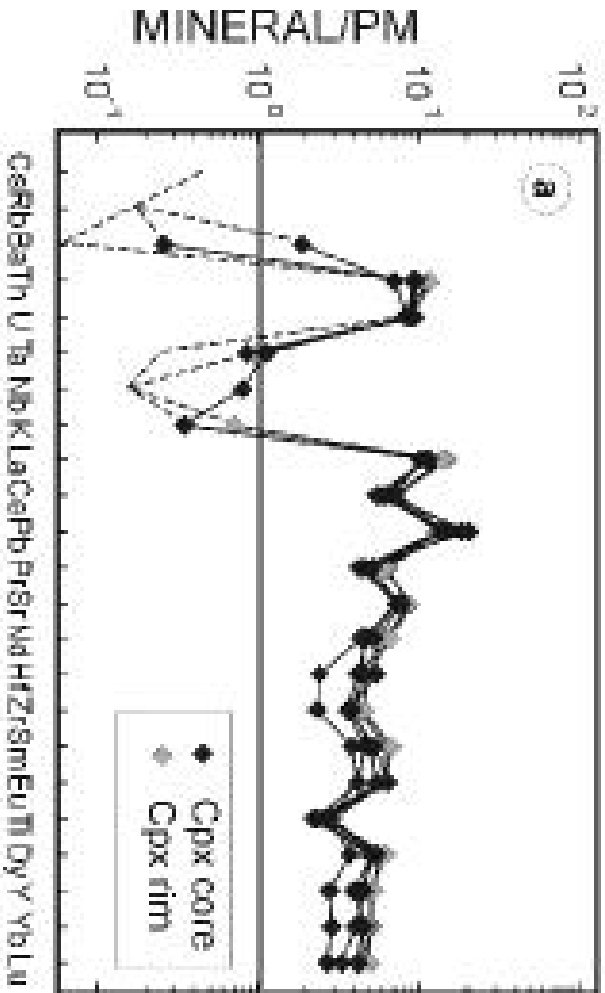
Microthermometry of H₂O - CO₂ inclusions

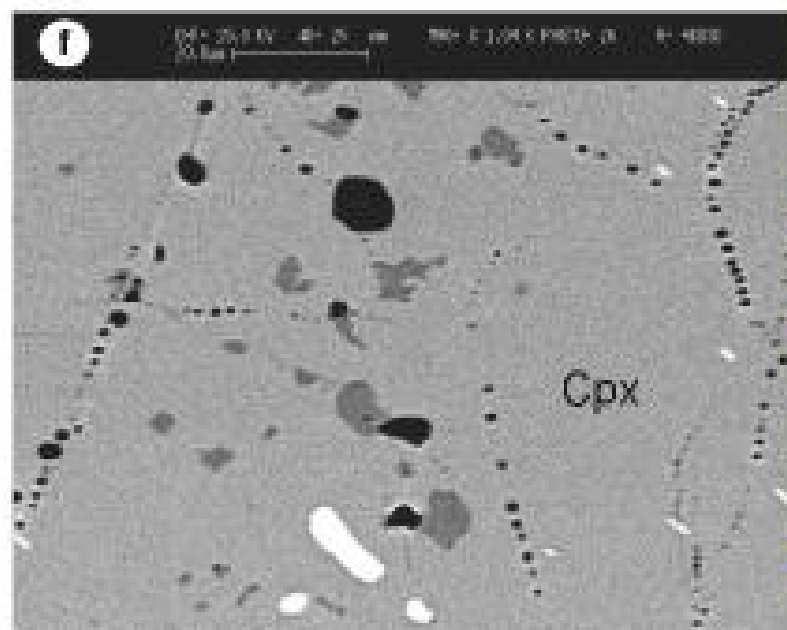
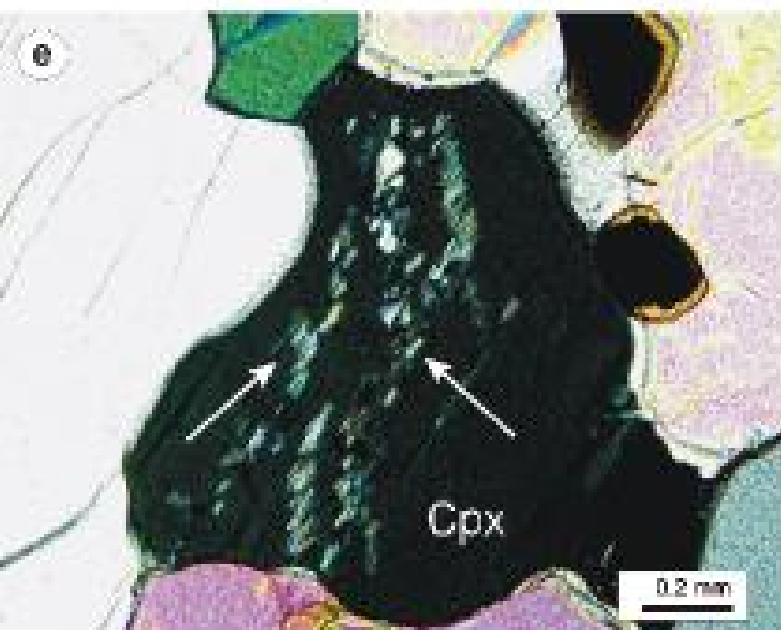
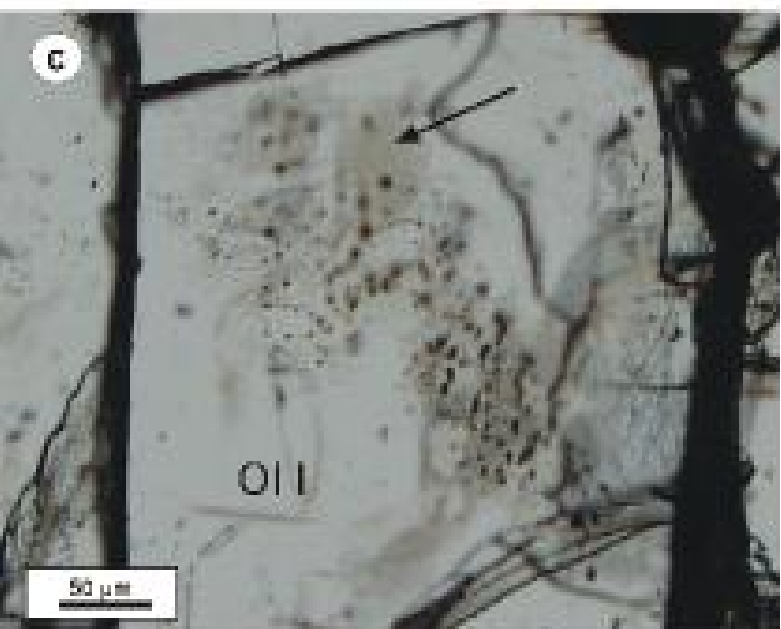
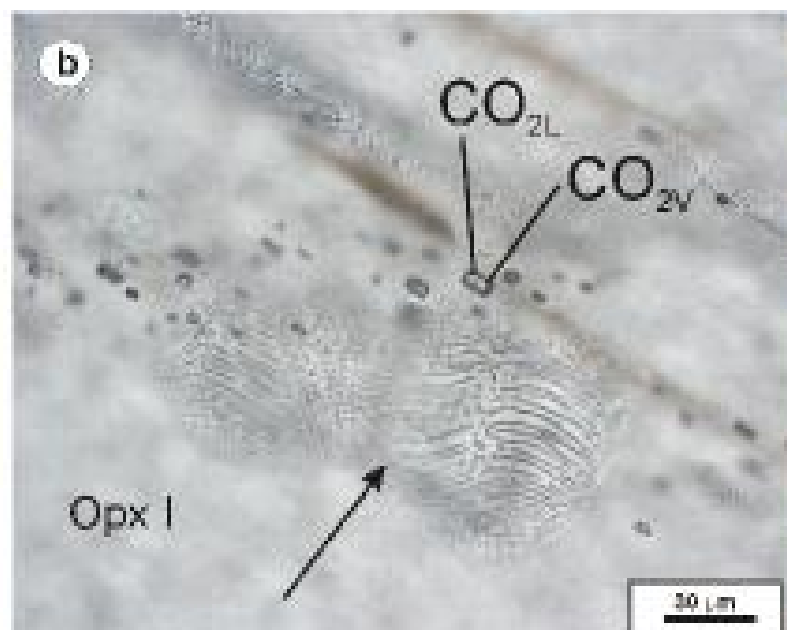
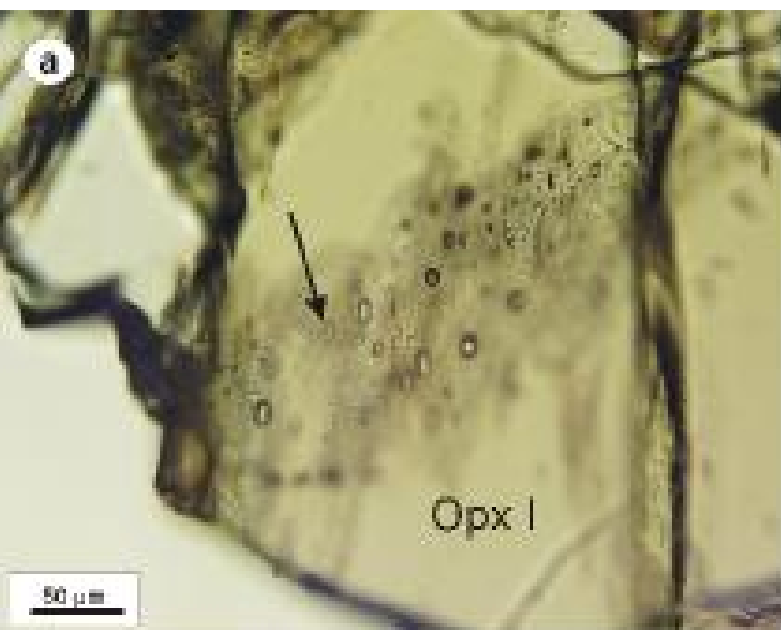
Sample	Host phase	Tf _{CO2} Tf°C	Tm _{CO2} °C	Th _{CO2} °C	Tf _{H2O} °C	Te °C	Tm _{Hhl} °C	Tm _{Clat} °C	Salinity NaCl eq.wt.%
INJ7/6A	Opx I	-89.2	-56.4	30.5	-51.3	-33.2	-11.3		
INJ7/6A	Opx I	-88.9	-56.4	27.2	-50.4	-31.6			
INJ7/7B	Opx I	-72.3	-56.3	6.4	-51.8	-30.7		5.6	10
INJ23/1A	OI I	-69.9	-57.6	24.2				2.7	14
INJ23/1A	OI I	-72.5	-56.7	24				2.7	14
INJ23/1A	OI I	-72.8	-56.7	23.9				2.7	14

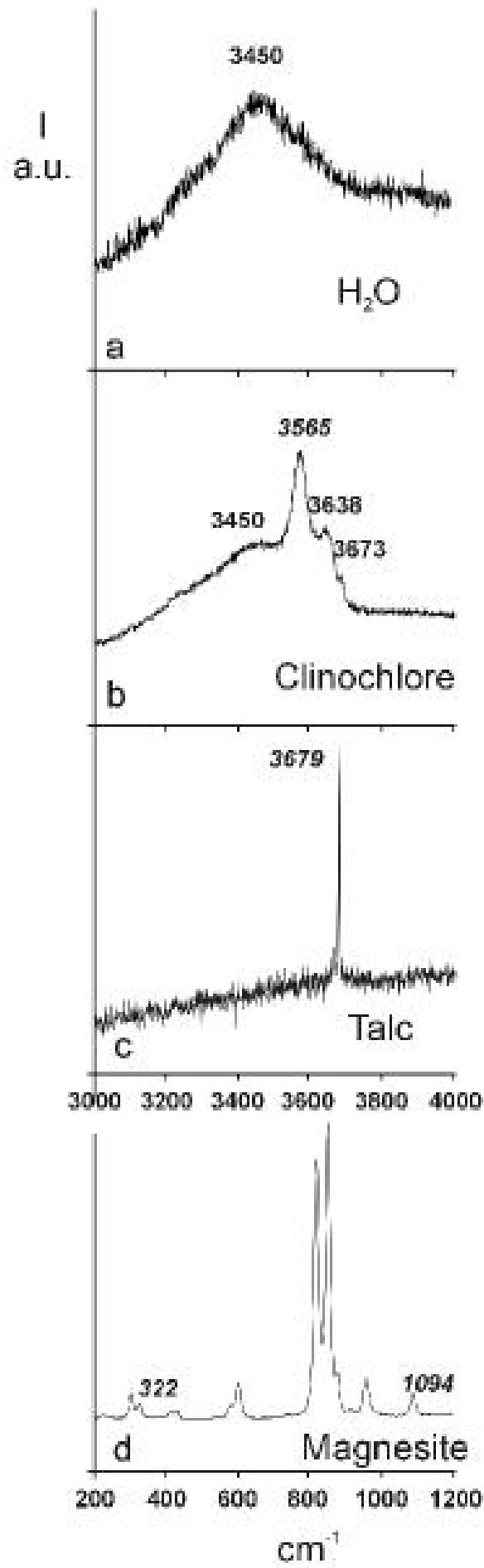
OI I: olivine porphyroclast; Opx I: orthopyroxene porphyroclast; Cpx: clinopyroxene; Microtherm.: Microthermometry; Tf = Temperature of freezing; Te = Eutectic Temperature; Tm = Temperature of melting; Th = Temperature of homogenization to the liquid phase; Hhl: hydrohalite; Clat = clathrate

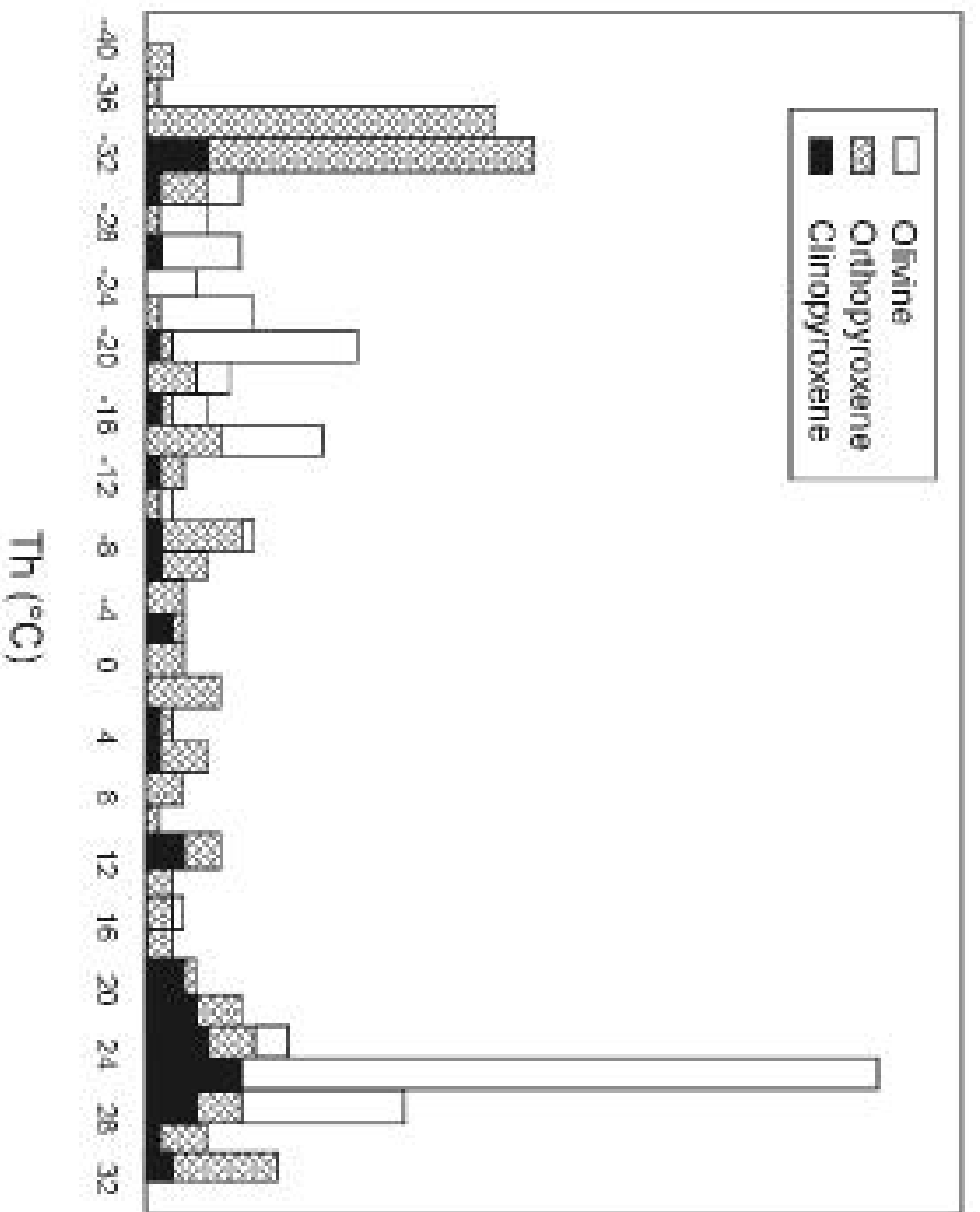


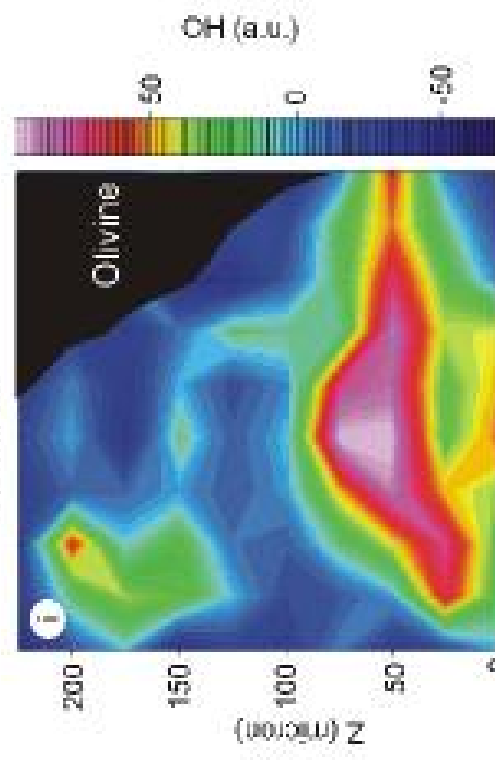
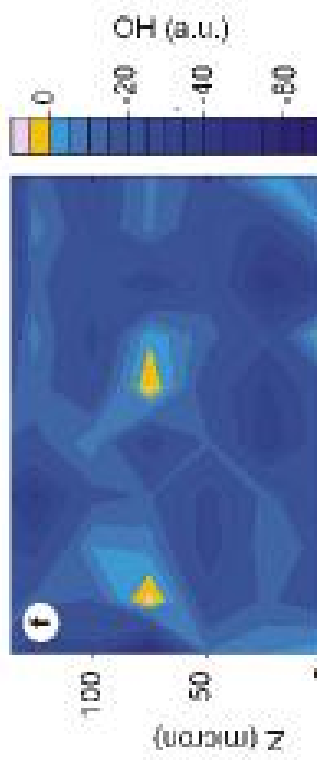
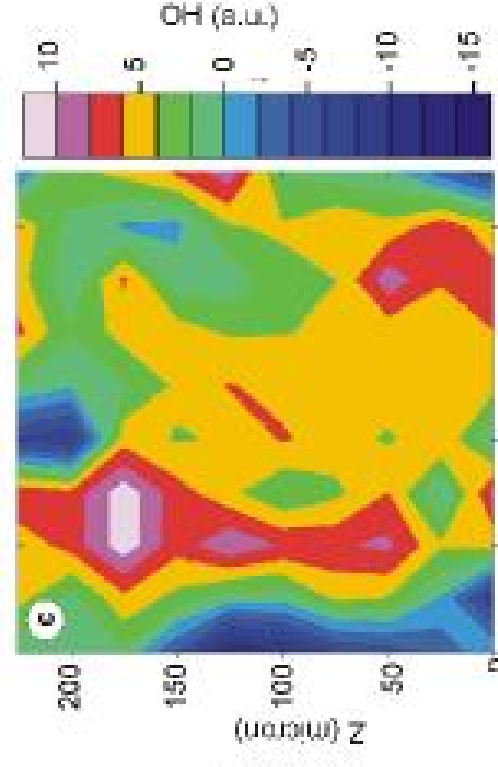
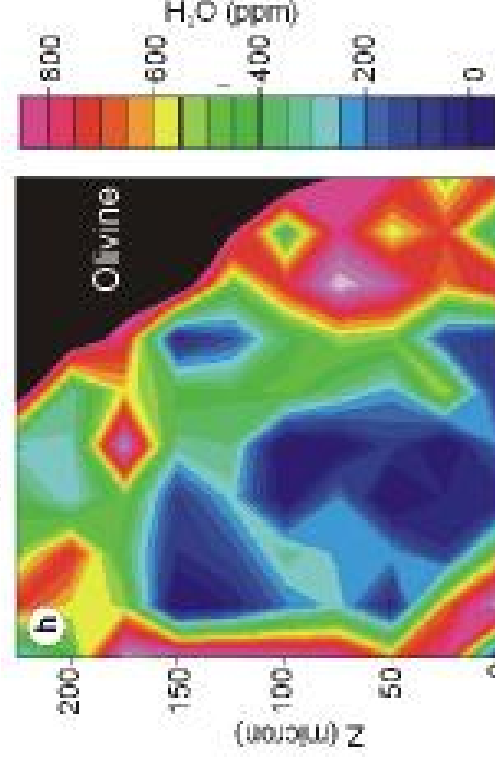
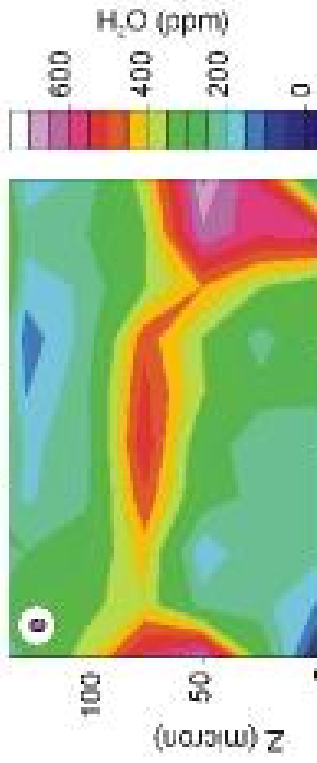
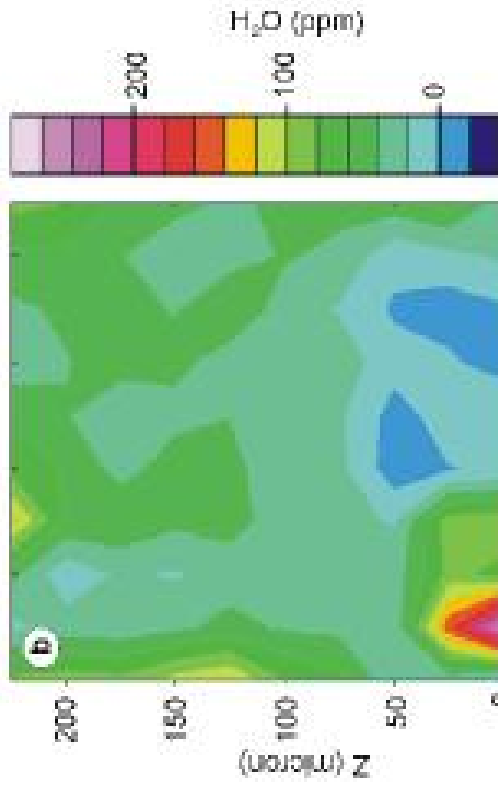
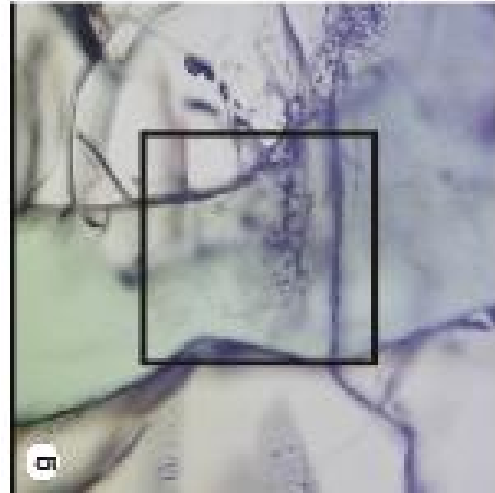
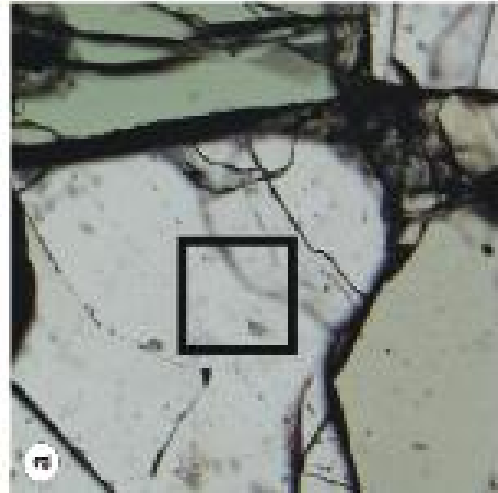












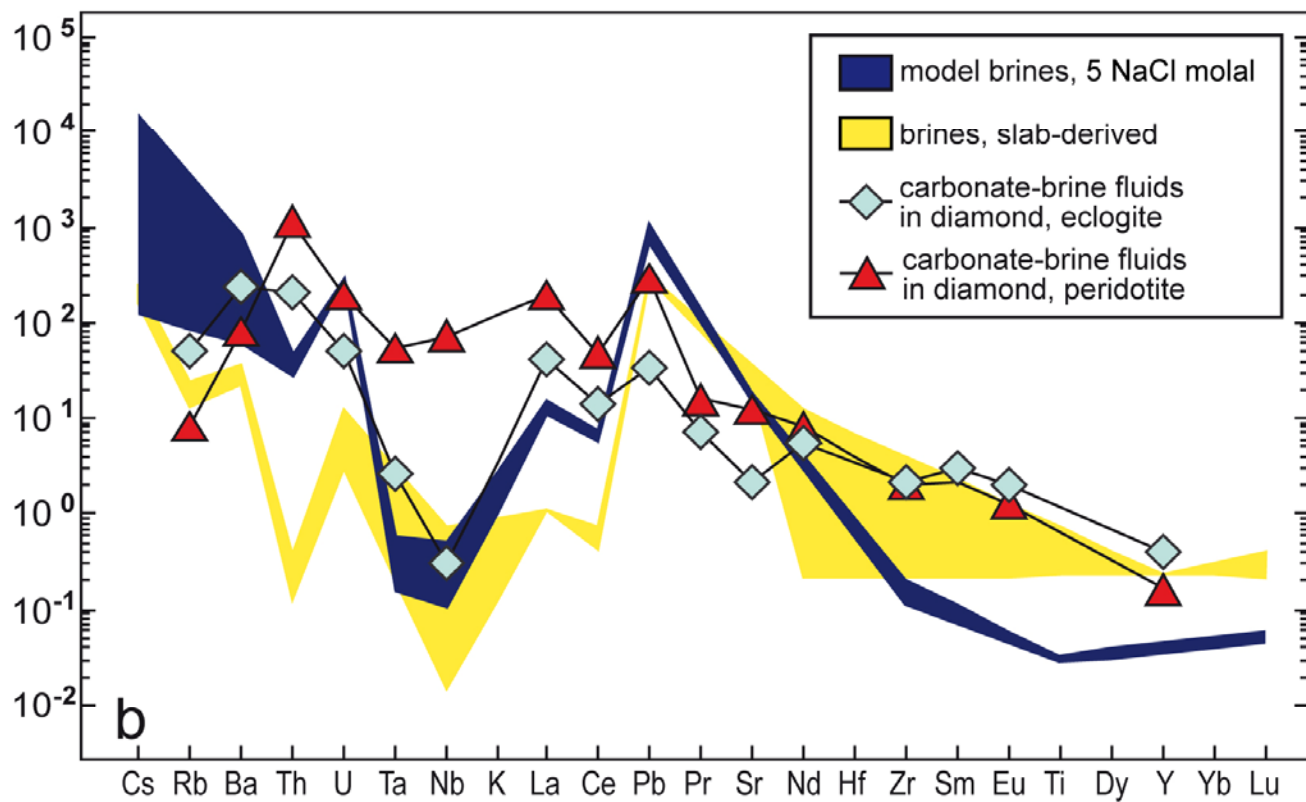
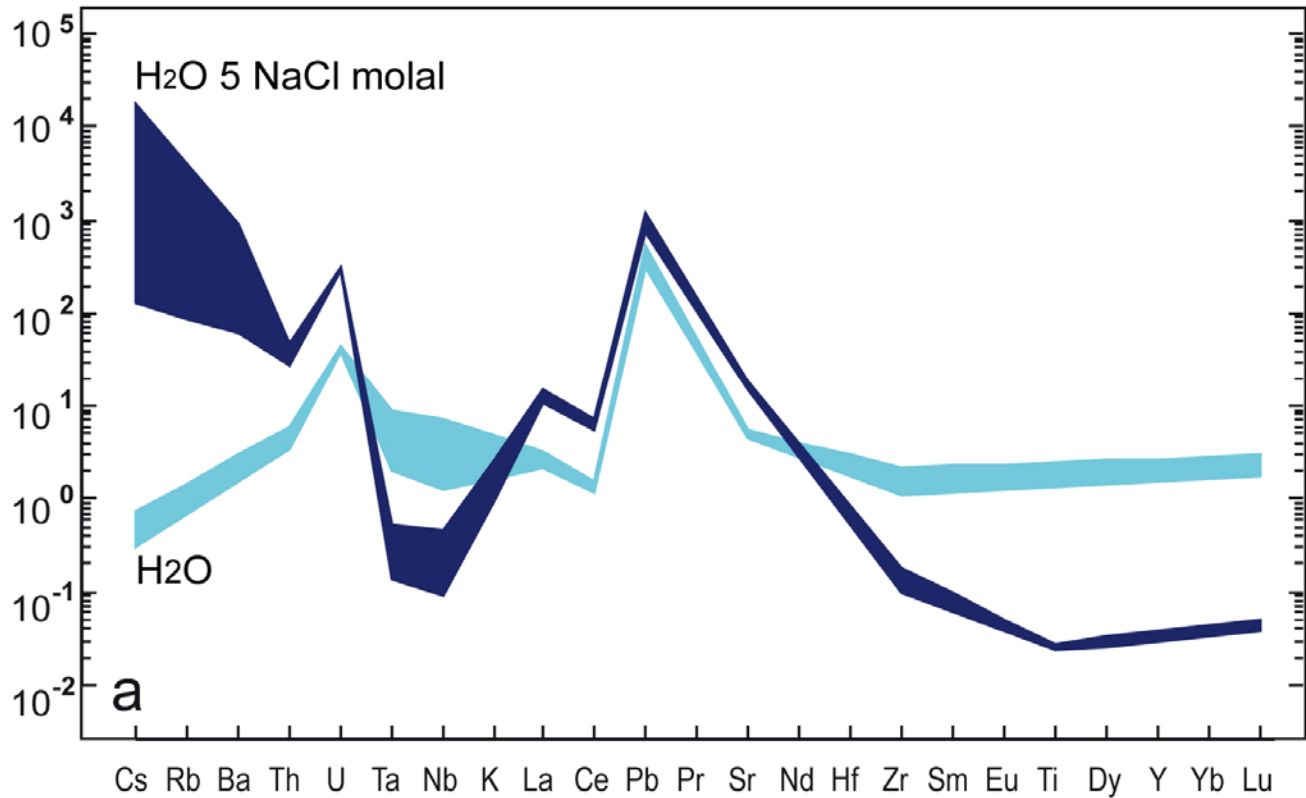


Fig. 8